LRP 454/92 April 1992

GEOMETRICAL AND PROFILE EFFECTS ON TOROIDICITY AND ELLIPTICITY INDUCED ALFVEN EIGENMODES

L. Villard & G.Y. Fu

submitted for publication to
Nuclear Fusion

GEOMETRICAL AND PROFILE EFFECTS ON TOROIDICITY AND ELLIPTICITY INDUCED ALFVEN EIGENMODES

L. VILLARD and G.Y. FU*

Centre de Recherches en Physique des Plasmas
Association Euratom - Confédération Suisse
Ecole Polytechnique Fédérale de Lausanne
21 Av. des Bains - 1007 Lausanne - Switzerland

* Present address : Plasma Physics Laboratory, Princeton University, P.O. Box 451, Princeton, New Jersey 08543, U.S.A.

ABSTRACT - The wave structures, eigenfrequencies and damping rates of toroidicity and ellipticity induced Alfvén eigenmodes (TAE, EAE) of low toroidal mode numbers (n) are calculated in various axisymmetric ideal MHD equilibria with the global wave finite element code LION. The importance of safety factor (q) and density (ρ) profiles on continuum damping rates is analysed. For realistic profiles several continuum gaps exist in the plasma discharge. Frequency misalignment of these gaps yields continuum damping rates γ/ω of the order of a few percent. Finite β_{pol} lowers the TAE eigenfrequency. For β values below the Troyon limit the TAE enters the continuum and can thus be stabilized. Finite elongation allows the EAE to exist but triangularity can have a stabilizing effect through coupling to the continuum. The localization of TAE and EAE eigenfunctions is found to increase with the shear and with n. Therefore large shear, through enhanced Landau and collisional damping, is a stabilizing factor for TAE and EAE modes.

1. INTRODUCTION

There has been a recent surge in the interest devoted to Alfvén eigenmodes induced by toroidicity (TAE) [1] and ellipticity (EAE) [2], since it was shown that these modes can be destabilized by energetic particles such as fusion alphas [3, 4, 11, 12]. Recent calculations predict TAE growth rates γ/ω of the order of 10^{-2} for planned thermonuclear burning experiments such as ITER [3]. Experiments conducted on TFTR [5] and DIII-D [6] tokamaks confirmed the existence of TAE modes and their destabilization by super-Alfvénic or slightly sub-Alfvénic particles obtained with neutral beam injection. No EAE mode was clearly identified in DIII-D as yet, in spite of the high elongation of this machine. One of the most critical issues to be resolved on the way to a fusion reactor is to evaluate the threshold for the instability. The threshold is determined by a balance between the kinetic instability growth rate due to energetic particles and the wave damping rate. In this paper we investigate in particular the possibility that continuum damping may be an important stabilizing factor for TAE and EAE modes. When continuum damping is absent direct electron Landau damping is evaluated. We calculate the strength of these dampings and single out the dependence on geometrical and profile parameters for the stabilization of these modes.

The present work focuses on the study of the spectrum of low n TAE and EAE modes for a variety of axisymmetric, low β, ideal MHD equilibria. Our global wave numerical approach allows us to obtain the complex eigenfrequency and eigenmode structure without making assumptions on smallness in inverse aspect ratio or elongation. Combined effects of toroidicity, ellipticity and triangularity can therefore be studied. Our method is not restricted to two-mode or three-mode coupling approximations. It can resolve the cases where one or more resonance surfaces are present. The calculations are performed using the finite element code LION [7].

Other works on the subject include an asymptotic theory to determine the continuum damping of high n TAE modes [8, 9]. Low n, fixed boundary TAE modes were already computed numerically in cases where no resonance surface is present in the plasma [1]. EAE modes were studied in Ref. [2] in the infinite aspect ratio limit. Continuum damping of n = 1 TAE modes was studied in Ref. [10] in the limit of large aspect ratio, with the approximation of two-mode and three-mode coupling, for the cases where only a single magnetic surface is resonant. More recently, fixed boundary TAE modes [27]

and their damping due to resonance absorption [28] were computed for the case of circular, finite aspect ratio tokamak plasmas.

This paper is structured as follows. A brief review of the spectrum of Alfvén modes and damping mechanisms is given in Section 2. In Section 3 we introduce the model and assess its relevance to the present study. The results are presented in Section 4 for a wide range of geometrical and profile parameters. Section 5 contains a discussion of the main results.

2. ALFVEN MODES AND THEIR DAMPING

2.1 Spectrum of Alfvén modes

Briefly, let us review the spectrum of Alfvén modes [15]. In cylindrical cold plasma theory, neglecting electron inertia [13], the spectrum contains Global Alfvén Eigenmodes (GAE) [14] and a continuum of shear Alfvén modes. The GAE wavefields have a global structure, whereas the continuum modes have a singularity at the spatial Alfvén resonance $\omega = \omega_A$, defined by $\omega_A = v_A k_{||}$, where v_A is the local Alfvén velocity and $k_{||}$ is the component of the wave number parallel to the equilibrium magnetic field $\vec{B}_0$. The GAE eigenfrequencies lie just below the corresponding continuum frequencies. If finite Larmor radius effects are taken into account, the continuum is replaced by a discrete set of damped eigenmodes of the kinetic Alfvén wave (KAW) [16].

The first radial mode is the most weakly damped and subsists in the cold plasma limit. It is therefore identified as a GAE. The real part of its eigenfrequency and its spatial structure depend very weakly on temperature. Unlike in the cold plasma model it has a small but finite imaginary part due to electron Landau damping and transit-time magnetic pumping. If electron inertia is included in the model, the spectrum contains also eigenmodes of the surface quasi-electrostatic wave (SQEW) [15]. Depending on the value of v_A/v_{te}, where $v_{te} = (2\, k_B T_e/m_e)^{1/2}$, resonance absorption is replaced by mode conversion to either the KAW ($v_A/v_{te} > 1$) or the SQEW ($v_A/v_{te} > 1$). When the mode converted waves are damped before reaching the plasma center or the edge, the total absorbed power in the plasma is the same as the cold plasma theory predicts.

In toroidal geometry, the finite aspect ratio couples poloidal wave numbers (m) with each other, and mainly m with the toroidal sidebands m ±

1. Thus, the eigenmodes of the system cannot be characterized by a single poloidal wave number. The effects of finite aspect ratio on the Alfvén wave spectrum are the following. The spatial Alfvén resonance condition ($\omega_A = v_A k_\parallel$) is now a differential equation involving the operator $\vec{B}_0 \cdot \nabla$ to be solved on a magnetic surface (ψ = const.) [15]. Let us define normalized units by setting the major radius of the magnetic axis $R_0 = 1$, the Alfvén velocity $v_{A0} = 1$, the equilibrium magnetic field $B_0 = 1$ and the mass density $\rho_0 = 1$ on magnetic axis. These units are used throughout the paper. Far from the regions where the different poloidal modes interact, in the limit $\omega << \omega_{ci}$, the resonance condition is approximately given by

$$\omega_A^2 = \frac{1}{\rho}\left(n + \frac{m}{q}\right)^2 \tag{1}$$

where n is the toroidal mode number and

$$q = q(\psi) = \oint \frac{1}{2\pi}\frac{1}{r}\frac{B_{ot}}{B_{op}}\, dl \tag{2}$$

In Eq. (2) B_{ot} and B_{op} are the toroidal and poloidal components of $\vec{B}_0$, respectively, and dl is a length element in the poloidal plane on a ψ = const. surface.

We note that the toroidal definition of q is used and not its cylindrical approximation. When the Alfvén frequencies of different m's come close to one another, Eq. (1) is no longer valid. The degeneracy of the continuum in a cylinder is removed by toroidal coupling. Gaps appear in the vicinity of the magnetic surfaces where

$$\left(n + \frac{m}{q}\right)^2 = \left(n + \frac{m+1}{q}\right)^2 , \tag{3}$$

thus where $q(\psi) = q_T$, with

$$q_T = \frac{|m| + \frac{1}{2}}{|n|} . \tag{4}$$

The frequencies of the centers of the toroidicity induced gaps are given approximately by

$$\omega_T = \frac{1}{2q_T\sqrt{\rho}} . \tag{5}$$

To first order in inverse aspect ratio (a/R) the gap size can be shown to be :

$$\omega_{\pm}^2 = \omega_T^2 \left(1 \pm 2 \frac{r_T}{R_0} \pm 2\Delta'(r_T)\right) \qquad (6)$$

where r_T is the minor radius of the magnetic surface $q = q_T$ and Δ is the Shafranov shift of the magnetic surface $q = q_T$.

Plasma ellipticity couples m components to the elliptical sidebands $m \pm 2$. The effect on the continuum is the creation of gaps in the vicinity of the magnetic surfaces $q(\psi) = q_E$, with

$$q_E = \frac{|m| + 1}{|n|} \quad . \qquad (7)$$

The frequencies of the centers of the ellipticity induced gaps are given approximately by

$$\omega_E = \frac{1}{q_E\sqrt{\rho}} \quad . \qquad (8)$$

It can be seen from Eqs (4) and (7) that the number of toroidicity and ellipticity induced gaps occurring simultaneously in the plasma discharge is proportional to $n(q_a - q_0)$, where q_a and q_0 are the values of q at the plasma boundary and on the magnetic axis, respectively. It therefore appears that TAE and EAE modes owe their existence to the coupling of more than two poloidal wave numbers m. The radial positions of the gaps depend on the q profile while their frequency overlap depends on the profile $1/q\sqrt{\rho}$.

Toroidicity and ellipticity have consequences on the spectrum of global Alfvén eigenmodes (GAE). It was shown [1] that global Alfvén eigenmodes can exist in the gaps of the continuum. They have been named toroidicity and ellipticity induced Alfvén eigenmodes (TAE and EAE, respectively), or "gap modes". Any Alfvén wave whose frequency is lower than the diamagnetic drift frequency of a super Alfvénic species can be driven unstable by resonant particle interactions [3, 4]. In future ignited plasmas TAE and EAE modes may be the best candidates for fusion alpha particle destabilization because of their relatively low frequency, as compared to the "cylindrical" GAE modes.

Another effect of toroidicity, combined to finite ω/ω_{ci}, is to allow the existence of a GAE in a region of the spectrum where none is expected from cylindrical theory. Experiments conducted on the TCA tokamak, as well as theoretical calculations performed with the LION code, showed the existence of a dominantly m = 0 GAE with an eigenfrequency just below the threshold of the m = 0 continuum [17].

2.2 Damping mechanisms

Toroidicity and other geometrical factors such as ellipticity and triangularity couple GAE, TAE and EAE modes to continuum modes of different poloidal wave numbers. Therefore these modes can have a resonance surface and be continuum damped. It was shown [18] that aspect ratios smaller than 10 are sufficient to stabilize the GAE modes. Cold plasma theory for a torus showed, in agreement with TCA results [21], the continuum damping rate of GAE modes to be of the order of a few percent of the wave frequency. In the case of TAE and EAE modes the presence of a resonance surface depends on q and ρ profiles, as suggested by Eqs (5) and (8). Multiple gap misalignment and geometrical coupling appear, thus, to be the basic mechanisms leading to the stabilization of TAE and EAE modes through continuum damping. Analytical calculations based on finite inverse aspect ratio expansion and asymptotic matching through the resonance [8, 9, 10] predicted continuum damping rates, when present, to be of the order of 10^{-2} of the mode frequency.

Finite Larmor radius and finite electron mass modifications of the Alfvén wave spectrum in torus have not been computed as yet. It is expected, by analogy with the cylindrical case, that the continuous spectrum is replaced by a discrete set of damped modes of the KAW and SQEW. The cylindrical results suggest that the total power absorbed is the same as given by the cold model when exciting a mode in the continuum. Therefore, the damping rates of the cold plasma global eigenmodes are not modified by kinetic effects in the cases where these modes have a resonance surface. The only possible exceptions would be when the mode converted waves reach the plasma center or edge before being damped so that global modes are set up. By analogy with the

cylindrical case, however, we assume that KAW and SQEW modes are more strongly damped than GAE, TAE and EAE modes. Therefore they should not be dangerous for stability.

When the cold plasma global modes have no spatial Alfvén resonance surface their damping rate must be evaluated with kinetic models. One of the candidates for damping in the TAE and EAE frequency range is electron Landau damping. For Alfvén modes, with $\omega \cong v_A k_{||}$, the local damping rate is given by [15]

$$\frac{\gamma}{\omega} = \frac{\sqrt{\pi}}{2} (k_\Lambda \hat{\rho}_i)^2 \frac{v_A}{v_{te}} \exp\left(- \frac{v_A^2}{v_{te}^2} \right) \qquad (9)$$

where k_Λ is the projection of the wavevector onto the plane perpendicular to $\vec{B}_0$, $\hat{\rho}_i$ is the ion Larmor radius evaluated with the electron temperature, $v_{te} = \sqrt{2k_B T_e / m_e}$. Equation (9) does not take into account trapped particles effects and thus probably over estimates the damping rate in the collisionless limit. However, collisions can enhance the damping due to trapped electrons. This is given approximately as [26] : $(\gamma/\omega)_{coll.} \approx 0.2 (k_\Lambda \hat{\rho}_i)^2 (\nu_e/\omega)^{1/2}$. Other damping mechanisms that could prove to be important for TAE and EAE modes are the following : (1) ion Landau damping, since v_A/v_{ti} is of the order of 2 to 3 in the center of a $T_i = 20$keV, $n_e = 4 \times 10^{20} m^{-3}$ reactor; (2) collisional damping and viscosity in the edge regions, especially in H-mode type discharges where edge density is relatively large and edge temperature relatively small and (3) magnetic curvature drift electron Landau damping, which is of the order of $\beta_e v_A / v_{te}$, where β_e is the ratio of electron pressure to magnetic field pressure. We emphasize the fact that all these dampings are proportional to k_Λ^2. Thus large gradients in the eigenfunction is a favourable condition to stabilize global eigenmodes.

3. PHYSICAL MODEL AND NUMERICAL METHOD

3.1 Equilibrium

All plasmas considered in this paper are assumed to be in axisymmetric ideal MHD equilibrium. The equilibrium magnetic field is written as $\vec{B}_0 = T\,\nabla\varphi + \nabla\varphi \times \nabla\psi$, where φ is the toroidal angle, ψ is the poloidal flux function, and $T = T(\psi)$ is the toroidal flux function. The poloidal flux function is a solution of the Grad-Shafranov equation

$$\nabla\left(\frac{1}{r^2}\nabla\psi\right) = -\frac{dP}{d\psi} - \frac{1}{2r^2}\frac{dT^2}{d\psi} \qquad (10)$$

where $P = P(\psi)$ is the plasma pressure. The equilibrium equation is solved numerically with the bicubic Hermite finite element code CHEASE [19]. The CHEASE code allows the specification of the aspect ratio, the shape of the plasma boundary, $P(\psi)$ and $T^2(\psi)$ profiles to be chosen in a wide variety of ways. In what follows, the functions $P(\psi)$ and $T^2(\psi)$ are expressed as polynomials. The CHEASE code proves to be highly accurate and has h^6 convergence properties, where h is the equilibrium mesh size. A single magnetic axis is assumed. The equilibrium is mapped onto toroidal coordinates (s, χ, φ). The "radial coordinate", s, is defined as $s = \sqrt{\psi/\psi_s}$, where ψ_s is the value of ψ at the plasma boundary. The "poloidal coordinate", χ, is chosen in such a way that the Jacobian J of the transformation from cartesian to toroidal coordinates is given by :

$$J = c(\psi) r^{\alpha} |\nabla\psi|^{\beta} \qquad (11)$$

where $c(\psi)$ is a normalization factor so that χ varies from 0 to 2π for each turn in the poloidal direction. The coefficients α and β in Eq. (11) can be set to $\alpha = 2$, $\beta = 0$, which generates a representation in which the magnetic field lines are straight, or to $\alpha = 1$, $\beta = 1$, which makes the poloidal coordinate χ proportional to the arc length around the magnetic surface in the poloidal direction.

3.2 Wave physics

We consider plasmas surrounded by a pure vacuum region enclosed by a perfectly conducting wall. The electromagnetic oscillations are excited by an antenna placed in this vacuum region. The antenna is modelled by a thin sheet on which surface currents $\vec{j}_a$ are prescribed with a $\exp(in\varphi - i\omega t)$ dependence, where n is an imposed toroidal mode number and ω an imposed frequency. The poloidal dependence of $\vec{j}_a$ can be chosen arbitrarily so long as $\vec{j}_a$ is kept divergence-free.

In the vacuum region we neglect the displacement current. In the frequency range of TAE and EAE modes the vacuum wavelength is much larger than the size of the machine. The equations in vacuum are simply

$$\vec{B} = \nabla\Phi \qquad \nabla^2\Phi = 0 \,. \tag{12}$$

Writing Maxwell's equations for the wave electric field $\vec{E}$ in the plasma we obtain, after linearization, and assuming a $\exp(in\varphi - i\omega t)$ dependence,

$$\nabla \times \nabla \times \vec{E} = \frac{\omega^2}{c^2} \vec{\vec{\varepsilon}} \cdot \vec{E} \tag{13}$$

where c is the vacuum velocity of light and $\vec{\vec{\varepsilon}}$ is the dielectric tensor operator. The cold, current-carrying plasma dielectric tensor, neglecting electron inertia, is used. In toroidal geometry, defining $\vec{e}_\psi = \nabla\psi / |\nabla\psi|$, $\vec{e}_\parallel = B_0/|B_0|$, $\vec{e}_\perp = \vec{e}_\parallel \times \vec{e}_\psi$, we have

$$\vec{\vec{\varepsilon}} \cdot \vec{E} = \begin{pmatrix} \varepsilon_{\psi\psi} & \varepsilon_{\psi\perp} \\ \varepsilon_{\perp\psi} & \varepsilon_{\perp\perp} \end{pmatrix} \begin{pmatrix} E_\psi \\ E_\perp \end{pmatrix} + \frac{c^2}{\omega^2} \frac{\vec{j}_0 \cdot \vec{B}_0}{B_0^2} (\nabla \times \vec{E})_\Lambda \tag{14}$$

where the subscript Λ denotes the projection in the $(\vec{e}_\psi, \vec{e}_\perp)$ plane, $\vec{j}_0$ is the equilibrium plasma current density, and

$$\varepsilon_{\psi\psi} = \varepsilon_{\perp\perp} = \frac{c^2}{v_A^2} \sum_i \frac{f_i}{1 - (\omega/\omega_{ci})} \tag{15a}$$

$$\varepsilon_{\psi\perp} = -\varepsilon_{\perp\psi} = i \frac{c^2}{v_A^2} \sum_i \frac{f_i \, \omega/\omega_{ci}}{1 - (\omega/\omega_{ci})^2} \tag{15b}$$

In the relations (15), ω_{ci} is the ion cyclotron frequency and f_i is the mass fraction of the ion species, $f_i = n_i m_i / \sum n_j m_j$; the summations are on all ions species. In this paper single ion species is considered. We note that ω/ω_{ci} does not play a significant role in the TAE and EAE frequency range. For $\omega << \omega_{ci}$ the dielectric tensor (Eq. (14)) is the same as the ideal MHD operator in which the adiabaticity index, γ_p, is set to zero. Ion acoustic waves cannot be described by this model. For low β plasmas considered in this work they have a much lower frequency than Alfvén waves. Moreover, they are strongly damped unless $T_e >> T_i$. They are therefore irrelevant for the present study.

The wave field solution of Eqs (13) (14) (15) exhibits singularities at the spatial Alfvén resonances on specific magnetic surfaces (ψ = const). The procedure to evaluate the corresponding resonance absorption is the following. A small imaginary part is added to the dielectric tensor : in Eqs (13) (14) (15) ω is replaced by

$$\omega(1 + i\nu), \ \nu > 0 \qquad (16)$$

The limit $\nu \rightarrow 0$ yields a finite absorption. The condition $\nu > 0$ is imposed to satisfy the causality principle. One of the most important features of resonance absorption is that it does not depend on the strength of the actual damping or detailed dissipation mechanism. The term ν in Eq. (16) should not be mistaken for the continuum damping rate $(\gamma/\omega)_{cont}$, which is finite even in the limit $\nu \rightarrow 0$. The relevance of the cold plasma resonance absorption model has been assessed by comparing it to the cylindrical hot plasma model that includes finite Larmor radius (FLR) effects [20] (see also section 2.2).

The damping rate of GAE modes experimentally observed in the TCA tokamak [21] is at least one order of magnitude larger than the prediction of the hot plasma cylindrical theory [22]. On the other hand, the cold plasma model in toroidal geometry predicts GAE damping rates in agreement with experiment. Even the toroidicity induced m = 0 GAE damping rate is correctly evaluated, at least in order of magnitude [17]. These results suggest that continuum damping due to toroidal effects, when present, is much larger than damping due to kinetic effects if toroidicity is neglected. Moreover, neither global modes of the KAW nor the SQEW have ever been observed in the experiment. This indicates that their damping in toroidal geometry is much larger than the hot plasma cylindrical theory predicts. The most effective damping mechanism for GAE modes appears thus to be toroidal coupling of

global modes to continuum modes. This mechanism is studied in this paper for TAE and EAE modes.

When an eigenmode has an eigenfrequency outside the continuum frequency range the cold plasma model is unable to predict its damping rate. Finite Larmor radius effects, entering mainly through electron Landau damping (see Eq. (9)), can be evaluated in the following way. For the small damping rates needed for TAE and EAE stabilization (γ/ω of the order 10^{-2}) we can assume, in the absence of mode conversion, that kinetic effects will not drastically modify the cold plasma eigenmode structure. In other words these effects have little influence on the dispersive properties of the wave, but mainly affect dissipation. Thus electron Landau absorption can be modelled by adding to $\varepsilon_{\psi\psi}$ (see Eq. (15a)) the term

$$\varepsilon_L = i \frac{c^2}{v_A^2} \sqrt{\pi}\, (k_\Lambda \hat{\rho}_i)^2 \frac{v_A}{v_{te}} \exp\left(-\frac{v_A^2}{v_{te}^2}\right) \tag{17}$$

where the value of k_Λ is evaluated by using the radial component of the eigenmode electric field, E_ψ, as calculated with the toroidal cold plasma model. The local damping rate is given by Eq. (9). The global damping rate can be obtained by

$$\left(\frac{\gamma}{\omega}\right)_L = \frac{\sqrt{\pi}}{2} \frac{\int \rho\, \hat{\rho}_i^2 \frac{v_A}{v_{te}} \exp\left(-v_A^2/v_{te}^2\right) |\nabla_\Lambda E_\psi|^2 d^3x}{\frac{1}{2}\int \rho\, |E_\psi|^2 d^3x} \tag{18}$$

where the integrals are on plasma volume.

3.3 Numerical method

Equations (13) - (16) are written in a weak variational form for a toroidal magnetic coordinate system (s, χ, φ) (see Section 3.1). A detailed expression of the weak form used can be found in Ref. [7].

The weak form is discretized using a non conforming linear finite element scheme [23]. The use of this discretization was mathematically shown

to avoid spectral pollution [24]. It is of crucial importance when the spectrum contains a continuous part. If a polluting method were used, spurious modes would appear in the discretized spectrum that could be mistaken for global modes, making the study of GAE, TAE and EAE modes unfeasible.

Since the spatial Alfvén resonances occur on ψ = const. surfaces, we see the obvious advantage of using a magnetic coordinate system. Moreover, the finite element scheme allows packing of the mesh around the resonance surfaces and gap positions where the wavefield is highly localized.

The vacuum equations, including relevant boundary conditions on the wall, matching conditions at the antenna, and continuity conditions at the plasma boundary, are solved with a Green's function technique. (More details can be found in Ref. [7].)

The wave field solution and the total power absorbed in the plasma, P, is then computed with the LION code. The numerical convergence properties of this code have been demonstrated in Ref. [7]. The total power, P, convergences at least as fast as h^2, where h is the computational mesh size.

The theoretical features of resonance absorption are well reproduced with the LION code. The limit $\nu \rightarrow 0$ (see Eq. (16)) is obtained numerically by studying the convergence properties of P with ν. In all cases we find a linear convergence property. Thus the value of the continuum absorption can be obtained even in cases of weak continuum damping.

A global eigenmode is found with the following method. The antenna current amplitude is kept constant and its driving frequency ω is varied. The response $P(\omega)$ is then computed with the LION code. A global mode, when excited, will show up as a peak. The position of the peak gives the real part of the eigenfrequency, $\mathrm{Re}\omega_0$. The half width at half maximum (HWHM) of the peak gives the imaginary part of the eigenfrequency, $\mathrm{Im}\omega_0$. The damping rate, γ/ω, is given by $\gamma/\omega = \mathrm{Im}\omega_0/\mathrm{Re}\omega_0$. Note that in order to obtain the HWHM correctly a convergence study must be made so that the limit $\nu \rightarrow 0$ can be obtained.

This method of finding the eigenfrequency and the eigenmode works only if the damping is small. For γ comparable to ω it is impossible to distinguish a peak on $P(\omega)$. However, for damping rates under consideration here, γ/ω of the order of 10^{-2} being sufficient to stabilize the alpha particle driven TAE and

EAE modes, our method is appropriate. The method fails only in cases where two global eigenmodes with the same toroidal wavenumber n have eigenfrequencies closer to one another than their damping rates. This is because the two peaks associated with each global mode merge and their HWHM cannot be calculated.

We point out that not just any arbitrary antenna current distribution can be used to excite a given global eigenmode. We have found that a good choice of antenna currents are those with helical distributions : $\vec{j}_a \sim \exp(im_a\theta + in\varphi)$, where θ is the poloidal angle. A "rule of thumb" is to use $m_a = -(n + 1)$ or $m_a = -(n + 2)$ to excite TAE and EAE modes. An important check of the validity of our method is to compare the eigenfrequencies, eigenmode structures and damping rates of the same eigenmode found with different antenna excitations : they are indeed the same.

The LION code can handle up to 50'000 mesh cells on a CRAY-1 type of computer. We find that 5'000 to 10'000 cells is a sufficiently fine mesh to evaluate TAE and EAE eigenfrequencies with an accuracy of a few percent, and their damping rates γ/ω with an accuracy of 10^{-3}. The LION code has been highly optimized : a computation with 5'000 mesh cells takes less than 20 s on a CRAY-2 computer.

The LION code computes the wavefield solution discretized in (s, χ) coordinates. The Fourier decomposition in χ is then performed as a diagnostic of this solution :

$$\vec{E}(s, \chi, \varphi, t) = \sum_m \vec{E}_m(s) e^{i(m\chi + n\varphi - \omega t)} \qquad (19)$$

This gives valuable insight into the toroidal, elliptical and triangularity coupling of different poloidal wavenumbers m. We find that the choice of the Jacobian with straight field line representation ($\alpha = 2$, $\beta = 0$ in Eq. (11)) gives a purer poloidal Fourier decomposition than the Jacobian with constant arc length ($\alpha = 1$, $\beta = -1$ in Eq. (11)). The straight field line Jacobian has the drawback that at high elongations the χ = const lines become too distorted. In such cases the constant arc length Jacobian was found to give more accurate results.

4. RESULTS

4.1 Density and safety factor profile effects

We first focus on the study of TAE modes in a $\beta = 0$ plasma of aspect ratio $R_0/a = 3.2$ having a circular cross-section. We examine the TAE spectrum for various q and ρ profiles. The value of q on magnetic axis, q_0, is kept constant with $q_0 = 1.05$, and the current density profile is changed in order to vary the value of q at plasma boundary, q_a. All q profiles considered in this paper are monotonic. The density profiles are specified by : $\rho = 1$ for $0 < s < 0.5$; for $0.5 < s < 1$, ρ is made a cubic function of s with $\rho(0.5) = 1$, $d\rho/ds(0.5) = 0$, $\rho(1) = 0.04$, $d\rho/ds(1) = -\alpha$. In varying the edge density gradient α, different ρ profiles are obtained (Fig. 1).

Figure 2 shows the total absorbed power versus applied frequency, $P(\omega)$, for the case $n = 1$, $q_a = 4.16$, $\alpha = 6$. Three TAE modes are excited at frequencies $\omega = .235$, .311, and .391. They are labelled (a), (b) and (c) in Fig. 2. Their continuum damping rates are $\gamma/\omega \cong 0.029$, 0., and 0.05, respectively. The corresponding eigenmode electric field structures are shown in Fig. 3. The labels (a), (b) and (c) in Fig. 3 correspond to the same labels as in Fig. 2. The left part of Fig. 3 displays level line plots of the real part of the radial electric field component, $Re(E_\psi)$, in the poloidal plane. The right part of Fig. 3 displays the real part of the poloidal electric field component, $Re(E_\perp)$. In Fig. 3 the particular structure of the constant-ReE_ψ and constant-$ReE_\perp$ lines in the vicinity of the magnetic axis comes from the fact that the electric wavefield has a $|m| = 1$ behaviour there. In the plasma of Fig. 3 three $n = 1$ toroidicity induced gaps exist simultaneously, for values of $q = q_T$ (Eq. (4)) given by $q_T = 1.5$, 2.5, 3.5. The corresponding m values are m = (-1, -2), (-2, -3), (-3, -4). The radial positions of the $q = q_T$ surfaces are $s = s_T = 0.6$, 0.87, 0.96, respectively. Let us first analyze the TAE mode labelled (b). This mode has no resonance surface and is not continuum damped. Its wavefield structure extends over the whole plasma cross-section. We note, however, that the electric field peaks around the magnetic surfaces $s = s_T$ where $q = q_T$. This localization of the wave field is much more apparent on the radial component of $\vec{E}$, $Re(E_\psi)$, (left side of Fig. 3) than on the poloidal component, $Re(E_\perp)$,

(right side of Fig. 3). This means that the gradients of the TAE electric field are dominated by the radial derivative of the radial component, $\frac{\partial E_\psi}{\partial s}$. In other words, $\vec{k}_\Lambda$, the projection of the wave vector of the TAE mode on the plane perpendicular to $\vec{B}_0$, is almost normal to the magnetic surfaces. The contributions to Landau damping, Eq. (18), come essentially from the 3 regions where the mode is localized, namely around $s = s_T = 0.6, 0.87, 0.96$, respectively. If we consider a deuterium plasma with a parabolic electron temperature profile with a central value of 2.5 keV, a central density $n_e = 3 \times 10^{19} m^{-3}$, $B_0 = 1T$, $R_0 = 2.4$ m, $a = 0.75$ m, which are typical parameters of the TAE excitation experiments on TFTR [5], we obtain a global electron Landau damping rate (Eq. (18)) of $(\gamma/\omega)_L \cong 4 \times 10^{-3}$. Around $s = 0.6, 0.87, 0.96$, we have $k_\Lambda \rho_i \cong 0.23, 0.16, 0.15$ and $v_A/v_{te} \cong 0.11, 0.18, 0.58$, respectively. We note that $k_\Lambda \rho_i$ is non negligible for the bulk deuterium ions. In a tokamak reactor $k_\Lambda \rho_\alpha$ will certainly be non negligible. This means that FLR and finite drift orbit size effects should be taken into account to investigate the wave-α particles interaction.

The poloidal Fourier decomposition, Eq. (19), of the TAE electric field shows a remarkable feature (Fig. 4b). Around $s = s_T = 0.6$, the Fourier components $m = -1$ and $m = -2$ dominate. But $s_T = 0.6$ is the radial position of the gap $q = q_T = 1.5$ created by the toroidal coupling of $m = -1$ and $m = -2$. The $q = q_T = 2.5$ surface is at $s = s_T = 0.87$, around which the toroidal coupling of $m = -2$ and $m = -3$ create a gap. This is also where the $m = -2$ and $m = -3$ components dominate the TAE structure. The $q = q_T = 3.5$ surface is at $s = s_T = 0.96$, around which the $m = -3, -4$ gap is located and where the $m = -3, -4$ components dominate the TAE structure. The TAE mode structure is thus a mixture of all poloidal wavenumbers m that have a gap in the plasma. This indicates that two-mode or three-mode approximations may not be accurate enough to determine the TAE spectrum, although locally around each gap position the corresponding two poloidal mode numbers m dominate. The particular TAE wave structures in the vicinity of $q = q_T$ surfaces found with the LION code agree with simple analytical theories in large aspect ratio, circular tokamaks. It can be shown analytically that the TAE Fourier components are approximately given by

$$E_{\psi m}(s) \propto \frac{\Delta_m + \alpha_m (s - s_T)}{(s - s_T)^2 + \Delta_m^2}, \quad E_{m\perp}(s) \propto \int_{s_T}^{s} E_{m\psi}(s) \qquad (20)$$

where s_T is the location of the $q = q_T$ surface, $\alpha_m = 0(1)$, and $\Delta_m \approx s_T^2/mSR$ (S is the shear). Then $k_\Lambda E_\psi \propto 1/\Delta_m \approx mSR/s_T^2$ which is proportional to n and the shear. The gap positions $s = s_T$ appear to be sufficiently accurately given by $q = q_T$ in Eq. (4), provided the toroidal definition of q is used (Eq. (2)) and not its cylindrical approximate. In the plasma of Fig. 3 the use of the q_{cyl} instead of q would have lead to a totally wrong conclusion for the gap structure. This suggests that the large aspect ratio limit is of restricted interest for the study of TAE modes in existing and future tokamak experiments.

In a torus, as was discussed in Section 2.1, the parallel wavenumber, $k_\parallel$, is a differential operator. Given the wavefield solution we can evaluate $k_\parallel$ for the TAE mode. Because of the particular poloidal structure described above, we find that $k_\parallel$ is everywhere almost equal to ω/v_A, where v_A is the local Alfvén velocity. Therefore $\omega/k_\parallel v_{te} \cong v_A/v_{te}$, and this justifies the use of Eqs (9) (17) (18) for the evaluation of Landau damping.

We should mention that the TAE modes shown in Fig. 3 have the property that the amplitude of E_ψ is a factor 3 to 10 larger than the amplitude of $E_\perp$. This corresponds to a plasma displacement $\vec{\xi}$ mainly in the poloidal direction. Therefore TAE modes are almost (but not totally) incompressible, hence the name "shear" or "torsional" Alfvén wave sometimes given to these modes.

Let us now examine the TAE mode labelled (a) in Figs 3 and 4. Its eigenfrequency, $Re\omega_0 = 0.235$, is below the lower m = -1, -2 gap edge, therefore it has *two* spatial Alfvén resonance surfaces at s = 0.5 and s = 0.65 with a mixture of m = -1, -2 poloidal behaviour there. We note a m = -2, -3 dominance around $q = q_T = 2.5$ and a m = -3, -4 dominance around $q = q_T = 3.5$, as was discussed for the TAE mode labelled (b). The continuum damping rate of this mode is $(\gamma/\omega)_{cont} \cong 0.029$. We remark that E_ψ (Fig. 3a left) is much more strongly peaked around the resonance surfaces than $E_\perp$ (Fig. 3a right). As a matter of fact, it can be shown that E_ψ has a $1/|s - s_{res}|$ singularity and $E_\perp$ has a $ln|s - s_{res}|$ singularity, in the limit $\nu \to 0$. This is reflected in the wavefield solution calculated with the LION code.

The TAE mode labelled (c) in Fig. 3 has its eigenfrequency, $Re\omega_0 = 0.391$, above the upper m = -2, -3 gap edge. Therefore it has *two* resonance surfaces at s = .84 and s = .89 with a dominant m = -2, -3 behaviour there. The same m dominances around $q_T = 1.5$ and $q_T = 3.5$ are observed as for the TAE mode labelled (b). This mode has a continuum damping rate $(\gamma/\omega)_{cont} \cong 0.1$.

The three TAE modes shown in Figs 3 and 4 are typical examples of all TAE modes found in this study although it may sometimes happen that the TAE mode has only one resonance surface close to the plasma boundary.

Let us now consider a sequence of ideal MHD equilibria keeping the same parameter as in Figs 2 - 4 except for q_a, the edge value of q. We use the same density profile characterized by an edge density gradient $\alpha = 6$. The eigenfrequencies and continuum damping rates of TAE modes versus q_a are shown in Fig. 5. It can be seen that the number of TAE modes for a given equilibrium depends on q_a. For $q_a < 3.75$ only one TAE mode persists. The others are either non-existent or very strongly damped (γ comparable to ω). The continuum damping rate of each TAE mode depends on the q profile. For example, between $q_a = 3.5$ and $q_a = 3.75$ the TAE mode is damped with a continuum damping rate of a few percent. This is due to the presence of the m = -3, -4 gap near the edge of the plasma. The density and q profiles are such that this gap is misaligned with the others and therefore the TAE mode has a resonance surface near the edge. It appears difficult to give an empirically simple rule for the dependence of damping rates of TAE modes on q profile. In all cases, however, this damping is due to a misalignment of the gaps.

The real part of the eigenfrequency of each TAE mode depends weakly on q_a (Fig. 5). But the eigenfrequency of the most weakly damped TAE mode does depend on q_a. For $2.89 \leq q_a \leq 3.98$ the most weakly damped TAE is the mode labelled (c), with $\Re e\omega_0 \cong 0.4$, whereas for $q_a > 4$ the mode labelled (b) is the most weakly damped, with $\Re e\omega_0 \cong 0.3$. Thus the frequency of the most weakly damped TAE decreases with increasing q_a.

We have conducted another study of the TAE spectrum versus q_a for the same sequence of equilibria as in Fig. 5, but with a different density profile characterized by an edge density gradient $\alpha = 4$. The same general conclusions hold but only details differ. The continuum damping rate of each TAE mode depends on q_a. The real part of the eigenfrequency of the most weakly damped mode is $\Re e\omega_0 \cong 0.44$ for $2.89 \leq q_a \leq 3.8$, and $\Re e\omega_0 \cong 0.32$ for $q_a > 3.8$. For $3.3 \leq q_a \leq 3.8$ the continuum damping rate is of the order of a few percent. This is due to the misalignment of the m = -3, -4 gap.

When still another density profile is used, characterized by an edge density gradient $\alpha = 0$, we find that all TAE modes are strongly damped,

$(\gamma/\omega)_{cont} > 0.1$, for all values of q_a considered. This is due to an even worse gap alignment.

Now let us study n = 2 and n = 3 TAE modes. In Fig. 6 we show the n = 2 TAE spectrum versus q_a for the density profiles characterized by $\alpha = 4$ and $\alpha = 6$. In almost all cases there is a finite continuum damping, $\gamma/\omega \geq 0.01$. We see that the continuum damping rate depends on q and ρ profiles in a non-obvious way. In Fig. 7 we show the continuum damping rates of the most weakly damped n = 2 and n = 3 TAE modes for a given q profile with $q_a = 2.89$ and different density profiles characterized by $0 < \alpha < 8$. In both cases there is an optimum value of α for which the continuum damping rate is minimal. These results can be interpreted as follows : the number of gaps in the plasma is proportional to n. As n increases it becomes more and more difficult to align all the gaps.

It should not be forgotten that these results have been obtained for a certain class of profiles. It is always possible, for a given q profile, to find a density profile for which the gaps are well aligned, even for n = 3. Let us now use a density profile $\rho(s) = (1 - .99s^2)^{0.7}$ and consider the same q profile as in Fig. 7, with $q_a = 2.89$. The $q = q_T$ (Eq. (4)) values for n = 3 are q_T = 1.167, 1.5, 1.833, 2.167, 2.5, 2.83. The corresponding radial gap positions $s = s_T$ are s_T = .42, .71, .84, .91, .96, .99, respectively. The frequencies of the centers of the gaps $\omega = \omega_T$ (Eq. (5)) are ω_T = .458, .424, .412, .422, .470, .64 respectively. Three n = 3 TAE modes were found, with $\Re e\omega_0$ = .430, .451, .506 and corresponding continuum damping rates of γ/ω = 0.03, 0.03, 0.004. The two first modes have several resonance surfaces with a mixture of m = -5, -6, -7, -8, -9 behaviour. The third one has its frequency near the edge of the m = -8, -9 continuum gap and thus has only weak continuum damping. Its electric wavefield structure is shown in Fig. 8. As for the n = 1 TAE modes, the wavefield extends over the whole plasma cross section and contains all poloidal modenumbers m that have a gap in the plasma. Around each gap position two poloidal mode numbers m dominate the Fourier decomposition. The radial component of the wave electric field, E_ψ, is much more localized than the poloidal component, $E_\perp$. It has a larger amplitude : $\max |E_\psi| / \max |E_\perp| \cong 3$. We note also that the wavefield radial localization is larger and larger as we go from the magnetic axis to the plasma boundary : the perpendicular wavenumber, k_Λ, increases with increasing shear, since the gap positions s_T are closer to each other as the shear increases.

In comparing the n = 1 and n = 3 cases (see Figs 3 and 8), we can see that k_Λ increases with n. The poloidal mode numbers m that enter into the composition of modes are proportional to n, as Eq. (4) suggests. Our results also indicate that the radial gradients of TAE modes increase with n. Therefore Landau damping increases with the shear and with n. For n = 3, q_a = 2.89 and a parabolic electron temperature profile with T_{eo} = 2.5keV, we estimate $(\gamma/\omega)_L \cong 1.35 \times 10^{-2}$. We found that FLR effects become more and more important as the shear and n increase. For circular plasmas of aspect ratio 3.2 and parabolic T_e profiles we found the electron Landau damping to follow approximately the semi-empirical scaling law

$$\left(\frac{\gamma}{\omega}\right)_L \approx 2.06 \times 10^{-3}\, n^2 (q_a - q_0)^2\, R_0^{-2}\, T_{eo}^{1/2}\, B_0^{-1}\, n_{eo}^{-1/2}\, A^{1/2} \qquad (21)$$

where n is the toroidal mode number, q_0 and q_a are the values of q on axis and on boundary, respectively, R_0 is expressed in meters, T_{eo} in keV, B_0 in Teslas, n_{eo} is the central electron density in units of $10^{19}m^{-3}$, and A is the ion mass in atomic units. Figure 9 shows $(\gamma/\omega)_L$ as calculated with the LION code versus $(\gamma/\omega)_L$ as evaluated with Eq. (21) for a wide variety of TAE modes. Agreement within 30% is obtained over two orders of magnitude. On the other hand, the driving term [3, 4] increases linearly with n, through the linear dependence of the drift frequency of fast particles, ω_{*f}, with m. Therefore there is an intermediate range of values of n that have the largest growth rate. Thus electron Landau damping is a possible mechanism that gives an upper limit on the toroidal wavenumbers n that may go unstable.

Electron Landau damping is most efficient where v_A is comparable to v_{te} and where the electron temperature is not too small. For typical existing or planned fusion tokamak experiments this occurs near the plasma boundary. Our results (Fig. 8) show that k_Λ is large in these regions and therefore electron Landau damping may effectively contribute to the global stabilization of TAE modes. Collisional damping also could be important in the edge regions of the plasma, where k_Λ is very large and the temperature is small.

4.2 Shafranov shift

Let us now examine the effect of Shafranov shift of magnetic surfaces on TAE modes. We use a sequence of equilibria of increasing β_{pol}, keeping $q_0 = 1.05$, $q_a = 2.89$, $\alpha = 4$, and the same geometrical parameters as in Figs 2 - 4. Figure 10 shows the n = 1 TAE frequency versus β_{pol} (thick line) and the lower edge of the m = -2, -3 continuum gap (thin line). The effect of Shafranov shift is to increase the gap size (see Eq. (6)). and to decrease the TAE frequency. The TAE frequency can be approximated by a linear function of β_{pol} :

$$\Re e\omega_0 \cong 0.44\ (1 - 0.5\ \beta_{pol}) \qquad (22)$$

For $\beta_{pol} \cong .85$ the n = 1 TAE enters the m = -2, -3 continuum and is subject to continuum damping for $\beta_{pol} > .85$. For $\beta_{pol} = .87$ we have $\beta = 1.5\%$. This corresponds to 84% of the Troyon β limit [25]. The TAE continuum damping rate is $\gamma/\omega = 0.027$. Thus the n = 1 TAE can be stabilized for β values below the ideal MHD stability limit.

4.3 Aspect ratio, elongation and triangularity effects

Let us consider a plasma of inverse aspect ratio a/R = .3125, $q_0 = 1.05$, $q_a = 2.89$, $\beta_{pol} = 0$, $\alpha = 4$, and study the spectrum of Alfvén eigenmodes as the ellipticity e is varied from 1 to 2. For all elongations the n = 1 TAE mode subsists and is not continuum damped. Its eigenfrequency decreases slightly with elongation and is approximately given by

$$\Re e\omega_0^{TAE} \cong 0.44\ (1 - 0.117(e - 1)^2) \qquad (23)$$

For $e \geq 1.5$ a new mode appears in the spectrum in the gap created by the coupling of m = -1 with m = -3 near $q = q_E = 2$ (Eq. (7)). It is an ellipticity induced Alfvén Eigenmode (EAE). Its continuum damping rate decreases rapidly with e. For e = 1.5, $(\gamma/\omega)_{cont} \cong 0.086$. For e = 2, $(\gamma/\omega)_{cont} \cong 0.002$. The real part of its eigenfrequency is $\Re e\omega_0^{EAE} \cong 1.24$. The EAE wavefield is localized near s = .9 where $q = q_E = 2$ (Eq. (7)) with a dominant m = -3 behaviour. It has

a dominant m = 0 resonance surface at s = .7. Coupling from m = -3 to m = 0 is weak and therefore the continuum damping is small. This is no longer the case if the plasma has some triangularity.

To analyze the effects of shaping we examine two sequences of equilibria of elongation 2 and varying aspect ratio. In the first sequence the triangularity, δ, is $\delta = 0$ and in the second $\delta = 0.3$. For all equilibria we keep $q_0 = 1.05$, $q_a = 2.89$, $\beta_{pol} = 0$, $\alpha = 4$. For a/R = 0.25, e = 2, $\delta = 0$, we show, in Fig. 11, the n = 1 continuum frequencies versus the radial coordinate s. The two toroidicity induced gaps around s = .78 ($q = q_T = 1.5$, m = -1, -2) and s = .975 ($q = q_T = 2.5$, m = -2, -3) are rather well aligned. The TAE has an eigenfrequency $\Re e\omega_0^{TAE} = 0.386$ and no continuum damping. The ellipticity induced gap near s = .92 ($q = q_E = 2$, m = -1, -3) is misaligned with the m = 0, -2 gap ($q = q_E = 1$) near s = 0. The EAE has an eigenfrequency $\Re e\omega_0^{EAE} = 1.228$ such that it has a dominantly m = 0 resonance surface at s = .72. However, toroidal coupling is small and triangularity coupling negligible, and the continuum damping rate is small : $(\gamma/\omega)_{cont} \cong 0.005$. The EAE has a dominant m = -3 and m = -1 behaviour near the ellipticity induced gap at s = .92. It is more localized in the edge region than the TAE.

The n = 1 TAE and EAE frequencies versus a/R are shown in Fig. 12 for the two cases $\delta = 0$ (continuous line) and $\delta = 0.3$ (dotted line). The frequencies of TAE and EAE modes increase slightly with a/R and δ. For all equilibria considered here the TAE mode is not continuum damped. The continuum damping rate of the EAE mode (see Fig. 13) shows a remarkable dependence on aspect ratio and triangularity. For $\delta = 0$ the damping increases quadratically with a/R, owing to the increase in the toroidal coupling of the dominantly m = -3 near $q = q_E = 2$ to the m = 0 resonant surface. For a given aspect ratio the EAE damping rate increases with triangularity. This can be understood by the fact that triangularity couples poloidal mode numbers m to $m \pm 3$. Thus it couples the dominantly m = -3 EAE wavefield near $q = q_E = 2$ to the dominantly m = 0 resonance surface. For $\delta = 0.3$ the EAE damping rate decreases with a/R. This result can be interpreted as follows. Increasing a/R changes the EAE frequency and the continuum in such a way that the distance between the $q = q_E = 2$ surface and the m = 0 resonance surface increases. This effect appears to be larger than the expected increase of toroidal coupling with a/R.

We conclude that triangularity is a stabilizing factor for the n = 1 EAE, but not for the n = 1 TAE.

Finite β_{pol} decreases the TAE and EAE frequencies. It can be expected that, for intermediate values of β_{pol}, the EAE frequency lies between the m = 0 and m = - 2 continua in the alignment of the gaps. Let us consider a plasma with a/R = .357, e = 2, δ = 0.4, q_0 = 1.05, q_a = 4.21, α = 4, β_{pol} = 0.5. In this case we find both an n = 1 TAE and an n = 1 EAE that have no resonance surface and thus no continuum damping. The n = 1 TAE has $\Re e\omega_0^{TAE} = 0.380$, and the n = 1 EAE $\Re e\omega_0^{EAE} = 1.002$.

The same equilibrium was used to study the n = 2 case. The n = 2 Alfvén spectrum contains a TAE mode with $\Re e\omega_0^{TAE} = 0.330$ and a EAE mode with $\Re e\omega_0^{EAE} = 0.973$, both of which are not continuum damped because their frequency lies in the gaps overlap. The n = 2 TAE electric field is shown in Fig. 14. The wavefield, particularly the radial component E_ψ, peaks around the $q = q_T$ surfaces, which are q_T = 1.25, 1.75, 2.25, 2.75, 3.25, 3.75. As in the circular case, the gradients of the eigenmode electric field are dominated by the radial gradients of E_ψ. The eigenmode structure appears to be asymmetric between the high-field side (HFS) and the low field side (LFS).

Figure 15 shows the n = 2 EAE electric field. It is even more asymmetric than the TAE. The wavefield amplitude is very small on the LFS of the plasma and very large on the HFS. In such an elongated and triangular cross-section the poloidal Fourier decomposition of the mode shows a mixture of many different poloidal mode numbers m.

Both TAE and EAE wavefields extend over the whole plasma cross-section. They have strong gradients in regions of high shear. Therefore we can expect TAE and EAE modes to be efficiently damped by electron Landau damping, since for typical reactor tokamak plasmas v_A is comparable to v_{te} near the edge where k_Λ and the mode amplitude are large. However, we could not find an expression similar to Eq. (21) for the damping rate. The reason is that TAE and EAE modes are particularly peaked near the boundary where $v_A \approx v_{te}$ and thus the damping rate strongly depends on details of T_e profile there.

The main difference between TAE and EAE modes, besides the higher EAE frequency, is that EAE continuum damping is more sensitive to the shape of plasma cross-section than the TAE. We conclude that it may be possible to stabilize EAE modes more easily by controlling the shape. The TAE mode thus appears to be the more dangerous mode in terms of stability.

For parameters of ITER we can assume that the density will be almost constant over the plasma cross-section except a small region near the edge.

Therefore we choose $q_0 = 1.05$, $q_a = 4.2$ and a constant density over the whole plasma cross-section. For this profile the toroidal gaps and the elliptical gaps are misaligned and both TAE and EAE modes are continuum damped. We show in Fig. 16 the n = 2 EAE wavefield. It has Alfvén resonance surfaces in the vicinity of the q = 3.5 and q = 4.0 surfaces with high poloidal wavenumbers. The continuum damping rate of this mode is $(\gamma/\omega)_{cont} \cong 5 \times 10^{-2}$. As a matter of fact the continuum damping rates of all n = 1 and n = 2 TAE and EAE modes for this "ITER" case are larger than or equal to 5×10^{-2}.

5. DISCUSSION

We have studied n = 1, 2, 3 TAE and n = 1, 2 EAE modes in more than 150 different axisymmetric plasma equilibria differing in safety factor and density profiles, poloidal β, aspect ratio, elongation and triangularity, in a parameter range relevant for present day and future tokamak experiments. Although this is not enough to provide definitive answers concerning these modes, in particular their possible stabilization through profile and shape control, we have found some important effects. The main results are summarized and discussed below.

- The existence of TAE and EAE modes in the presence of multiple gaps is confirmed. All poloidal mode numbers m that have a corresponding gap are present in the wavefield structure. The TAE and EAE wavefields extend over the whole plasma cross-section and their amplitude peaks on all gap positions. See Figs 3, 8, 14, 15 and 16.
- We have evidenced the multiplicity of TAE modes (see Figs 2 - 5). The eigenmode frequency split appears to be non negligible and seems to be a regular feature of TAE spectra. Other examples of this split can be found in Ref. [28].
- Continuum damping is an important stabilizing mechanism. When present it is roughly a few percent of the mode frequency. See Figs 5, 6, 7 and 18.
- The continuum damping rate is controlled by multiple gaps misalignment, which depends on q and ρ profiles. For example, for a given q profile, hollow ρ profiles with steep edge gradients ($\alpha = 8$) or peaked ρ profiles with flat edge gradients ($\alpha = 0$) yield continuum damping rates of several percent (Fig. 7).
- We could not find any clear dependence of the continuum damping rate on n. High n cases cannot be studied with the LION code : for realistic q

profiles the number of gaps becomes too large to be resolved numerically. Therefore a comparison with the results of Refs [8, 9], where a decrease of the continuum damping rate with n was found, cannot be made. For the low n cases studied here, the sensitivity of the continuum damping rate on minor changes of q and ρ profiles (see Figs. 5 - 7) makes a study of the n dependence irrelevant at low n.

- Finite β_{pol} can stabilize the n = 1 TAE for β values below the Troyon limit (Fig. 10).
- The real part of eigenfrequencies of TAE and EAE modes do not depend much on q_a or n (Fig. 5). For TFTR parameters [4] TAE frequencies are in the range of 60 to 100 kHz, which agrees well with experiment.
- The amplitude of the radial electric field, E_ψ, for both TAE and EAE modes is much larger than the amplitude of poloidal electric field, $E_\perp$.
- The radial gradients of TAE and EAE wavefield component E_ψ are much larger than radial gradients of $E_\perp$. In other words, the perpendicular wavenumber, k_Λ, of TAE and EAE modes is mainly due to the large $\partial E_\psi/\partial s$.
- Increasing shear increases k_Λ. Thus, in the absence of continuum damping, large shear is a stabilizing factor for both TAE and EAE modes through enhanced kinetic damping.
- Landau damping of TAE and EAE modes increases quadratically with n through increased eigenmode gradients (see Eq. (21) and Fig. 9). Since the fast particle instability growth rate increases linearly with n, this implies that low or intermediate toroidal mode numbers are the most easily destabilized. This agrees well with experiments on DIII-D and TFTR.
- The parallel wavenumber, $k_\parallel$, of TAE and EAE modes is accurately given by ω/v_A. It simplifies the expressions for wave-particle interaction such as Landau damping which therefore depends only on the profiles of v_A/v_{te}, Te and eigenmode gradients ($\partial E_\psi/\partial s$).
- The radial positions of the gaps are well predicted by the simple expressions $q = q_T$ (Eq. (4)) and $q = q_E$ (Eq. (7)) when the exact toroidal definition of q is used (Eq. (2)). These are the positions where the eigenmode peaks, especially the radial electric field component E_ψ. This emphasizes the importance of studying TAE and EAE modes in exact toroidal ideal MHD equilibria.

- The large k_Λ values for TAE and EAE modes imply that FLR and finite drift orbit width effects should be taken into account to study wave-fast particles interactions.
- Triangularity and small aspect ratio can be stabilizing factors for EAE modes in elongated plasmas (see Fig. 13). On the other hand, TAE modes are more robust and are therefore more dangerous for stability than EAE modes. This seems to contradict the conclusions of Ref. [2]. The contradiction is, however, only apparent. Our conclusion results from the combined effects of triangularity and finite aspect ratio (both of which were neglected in Ref. [2]) with ellipticity. Our results for large aspect ratio and zero triangularity (Fig. 13) confirm the conclusions of Ref. [2] : continuum damping of EAE is very small.
- The TAE frequency decreases with β_{pol} (see Fig. 10 and Eq. (22)) and with elongation (see Eq. (23)). This could explain the lower frequencies observed in DIII-D [6], although some other effects, such as toroidal rotation, seemed to play a role in these experiments but were not studied here.
- Although no optimization of antenna design was made in the present work, we have shown that TAE and EAE modes can be excited with an antenna placed in the vacuum region. This might be an experimentally feasible and interesting way to study the global damping rate of these modes.
- H-mode like profiles in plasmas with a separatrix ($q \to \infty$) cannot be studied with the present version of the LION code. However, if the density profile is flat, a non-uniform $1/q\sqrt{\rho}$ profile is generated and therefore leads to toroidicity and ellipticity gap misalignments. For ITER parameters we found continuum damping rates of all $n = 1$ and $n = 2$ TAE and EAE modes larger than or equal to 5×10^{-2}.

6. CONCLUSION

Our study has shown how continuum damping is a critical stabilizing factor for TAE and EAE modes. We have exposed important parameters such as q and ρ profiles, aspect ratio, elongation and triangularity which influence it. For reasonable profiles, low n TAE and EAE modes are effectively continuum-damped in ITER-like plasmas. The authors of Refs [8, 9] have pointed out that continuum damping is less efficient at high n. However, provided the n^2 dependence of electron Landau damping that we propose in

this paper still holds, high n modes might be effectively damped by this mechanism. Therefore intermediate n modes should be the most dangerous for stability, in good agreement with experimental results so far [4, 5].

More work is necessary to make a reliable prediction of TAE and EAE stability in future reactor devices. In particular FLR and finite drift orbit size effects should be considered for a better estimate of wave-α particle interactions. The radially fine eigenmode structure in the regions of high shear near the plasma edge suggests that interaction with turbulence might also play an important role. Continuum damping and electron Landau damping usually act in the outer regions of the plasma more effectively than in the center. It can therefore be expected that in a reactor TAE or EAE modes would be locally unstable in the vicinity of the magnetic axis but locally stable in the outer regions. Even when globally stable, TAE or EAE modes might carry a non negligible energy flux from the center to the outer regions.

ACKNOWLEDGEMENTS

The authors would like to thank Drs J. Vaclavik and K. Appert for fruitful discussions, H. Lütjens for providing the equilibrium code CHEASE and R.D. Parker for reading the manuscript.

This work was partly supported by the Swiss National Science Foundation.

REFERENCES

[1] CHENG, C.Z., CHANCE, M.S., Phys. Fluids **29** (1986) 3695.
[2] BETTI, R., FREIDBERG, J.P., Phys. Fluids B **3** (1991) 1865.
[3] FU, G.Y., VAN DAM, J.W., Phys. Fluids B**1** (1989) 1949.
[4] CHENG, C.Z, Phys. Fluids B **3** (1991) 2463.
[5] WONG, K.L., FONCK, R.J., PAUL, S.F. et al., Phys. Rev. Lett. **66** (1991) 1874.
[6] HEIDBRINK, W.W., STRAIT, E.J., DOYLE, E., SAGER, G., SNIDER, R.T., Nucl. Fusion **31** (1991) 1635.
[7] VILLARD, L., APPERT, K. GRUBER, R., VACLAVIK, J., Comput. Phys. Rep. **4** (1986) 95.
[8] ROSENBLUTH, M.N., BERK, H.L., VAN DAM, J.W., LINDBERG, D.M., Phys. Rev. Lett. **68** (1992) 596.
[9] ZONCA, F., CHEN, L., Phys. Rev. Lett. **68** (1992) 592.
[10] BERK, H.L., VAN DAM, J.W., GUO, Z., LINDBERG, D.M., Continuum damping of low-n toroidicity-induced shear Alfvén eigenmodes, Rep.

IFSR 499, Institute for Fusion Studies, The University of Texas, Austin (1991).
[11] FU G.Y., VAN DAM, J.W., Excitation of toroidicity-induced shear Alfvén eigenmode by fusion alpha particles in an ignited tokamak, Rep. ISFR 368, Institute for Fusion Studies, The University of Texas, Austin (1989).
[12] VAN DAM, J.W., FU G.Y., CHENG C.Z., Thermonuclear instability of global-type shear Alfvén modes, Rep. IFSR 413, Institute for Fusion Studies, The University of Texas, Austin (1990).
[13] APPERT, K., VACLAVIK, J., VILLARD, L., Phys. Fluids **27** (1984) 432.
[14] APPERT, K., GRUBER, R., TROYON, F., VACLAVIK, J., in Heating in Toroidal Plasmas, (Proc. 3rd Joint Varenna-Grenoble Int. Symp. Grenoble, 1982), Vol. 1, CEC, Brussels (1982) 203.
[15] VACLAVIK, J., APPERT, K., Nucl. Fusion **31** (1991) 1945.
[16] HASEGAWA, A., CHEN, L., Phys. Rev. Lett. **35** (1975) 370.
[17] APPERT, K., COLLINS, G.A., HOFMANN, F. et al., Phys. Rev. Lett. **54** (1985) 1671.
[18] CHENG, C.Z., FU, G.Y., VAN DAM, J.W., in Theory of Fusion Plasmas (Proc. of the Joint Varenna - Lausanne Int. Workshop, Chexbres, Switzerland, 1988), Editrice Compositon Bologna (1988) 259.
[19] LUETJENS, H., BONDESON, A., ROY, A., Comput. Phys. Commun. **69** (1992) 287.
[20] APPERT, K., HELLSTEN, T., VACLAVIK, J., VILLARD, L., Comput. Phys. Commun. **40** (1986) 73.
[21] COLLINS, G.A., HOFMANN, F., JOYE, B., KELLER, R., LIETTI, A., LISTER, J.B., POCHELON, A., Phys. Fluids **29** (1986) 2260.
[22] APPERT, K., HELLSTEN, T., LUETJENS, L., SAUTER, O., VACLAVIK, J., VILLARD L., in Plasma Physics (Proc. 7th. Int. Conf. Kiev, 1987), Invited Papers, Vol. 2, World Scientific, Singapore (1987) 1230.
[23] GRUBER, R., RAPPAZ, J., Finite Element Methods in Linear Ideal Magnetohydrodynamics, Springer-Verlag, Berlin (1985).
[24] RAPPAZ, J., Numer. Math. **28** (1977) 15.
[25] TROYON, F., GRUBER, R., Phys. Letters **110A** (1985) 29.
[26] MAZUR, V.A., MIKHAJLOVSKIJ, A.B., Nucl. Fusion **17** (1977) 193.
[27] TURNBULL, A.D., CHU, M.S., CHANCE, M.S., GREENE, J.M., LAO, L.L., STRAIT, E.J., Toroidicity-Induced Alfvén Eigenmodes in Low Aspect Ratio Tokamaks, Rep. GA-A20746, General Atomics, San Diego (1992), submitted to Phys. Fluids B.
[28] POEDTS, S., KERNER, W., GOEDBLOED, J.P., KEEGAN, B., HUYSMANS, G.T.A., SCHWARZ, E., Damping of Global Alfvén Waves in Tokamaks due to Resonant Absorption, Rep. JET-P(92)03, JET Joint Undertaking, Abingdon (1992), submitted for publication to Plasma Phys. & Contr. Fusion.

FIGURE CAPTIONS

FIG. 1. Density profiles parametrized with the value of the edge gradient α.

FIG. 2. Power vs frequency for n = 1, in a circular tokamak of aspect ratio 3.2, $q_0 = 1.05$, $q_a = 4.16$, $\alpha = 6$, $\beta = 0$. Three gap modes, labelled (a), (b) and (c), are found. Their eigenmode structures are shown in Figs 3 - 4.

FIG. 3. Level line plots of n = 1 TAE electric fields. The labels a (top), b (middle) and c (bottom) correspond to those in Fig. 2. The constant

$\Re_e(E_\psi)$ (left side) and constant $\Re_e(E_\perp)$ (right side) lines are colour-coded with blue for low values to red for high values.

FIG. 4. Poloidal Fourier decomposition of the TAE modes shown in Fig. 3. The labels a, b and c correspond to those in Figs 2 and 3.

FIG. 5. Frequencies and damping rates of n = 1 TAE modes versus q_a. The other parameters are R/a = 3.2, q_0 = 1.05, α = 6, β = 0, circular cross-section.

FIG. 6. Frequencies and damping rates of the most weakly damped n = 2 TAE modes versus q_a, for density profiles characterized by α = 4 (continuous line) and α = 6 (dotted lines). The other parameters are R/a = 3.2, q_0 = 1.05, α = 6, β = 0, circular cross-section.

FIG. 7. Damping rates of the most weakly damped n = 2 and n = 3 TAE modes for different density profiles. The other parameters are R/a = 3.2, q_0 = 1.05, β = 0, circular cross-section.

FIG. 8. Level line plots of n = 3 TAE electric field in a circular tokamak with q_0 = 1.05, q_a = 2.89, $\rho(s) = (1 - .99s^2)^{0.7}$, β = 0. The colour coding is the same as in Fig. 3.

FIG. 9. Global electron Landau damping rate of TAE modes as calculated with the LION code versus the semi-empirical formula, Eq. (21), for circular plasmas of aspect ratio 3.2 and parabolic electron temperature profiles.

FIG. 10. Frequency of the n = 1 TAE mode (thick line) versus β_{pol}, in a circular tokamak with R/a = 3.2, q_0 = 1.05, q_a = 2.89, α = 4. The thin line shows the lower edge of the continuum gap.

FIG. 11. Continuum frequencies versus radial position s in a plasma of aspect ratio 4, elongation 2, triangularity 0, q_0 = 1.05, q_a = 2.89, α = 4, β = 0. The numbers on the curves correspond to the dominant poloidal mode numbers m.

FIG. 12. Frequencies of n = 1 TAE and EAE modes versus inverse aspect ratio in plasmas of elongation 2, triangularity 0 (continuous lines) and triangularity 0.3 (dotted lines). The other parameters are q_0 = 1.05, q_a = 2.89, α = 4, β = 0.

FIG. 13. Damping rates of n = 1 EAE modes versus inverse aspect ratio in plasmas of elongation 2, triangularity 0 (continuous line) and triangularity 0.3 (dotted line). The other parameters are q_0 = 1.05, q_a = 2.89, α = 4, β = 0.

FIG. 14. Level line plot of the n = 2 TAE electric field in a plasma of inverse aspect ratio 2.8, elongation 2, triangularity 0.4, q_0 = 1.05, q_a = 4.21, β_{pol} = 0.50, α = 4. The colour coding is the same as in Fig. 3.

FIG. 15. Level line plot of the n = 2 EAE electric field. Same parameters as in Fig. 14.

FIG. 16. Level line plot of the n = 2 EAE electric field. Same parameters as in Fig. 14 except the density profile which is uniform here.

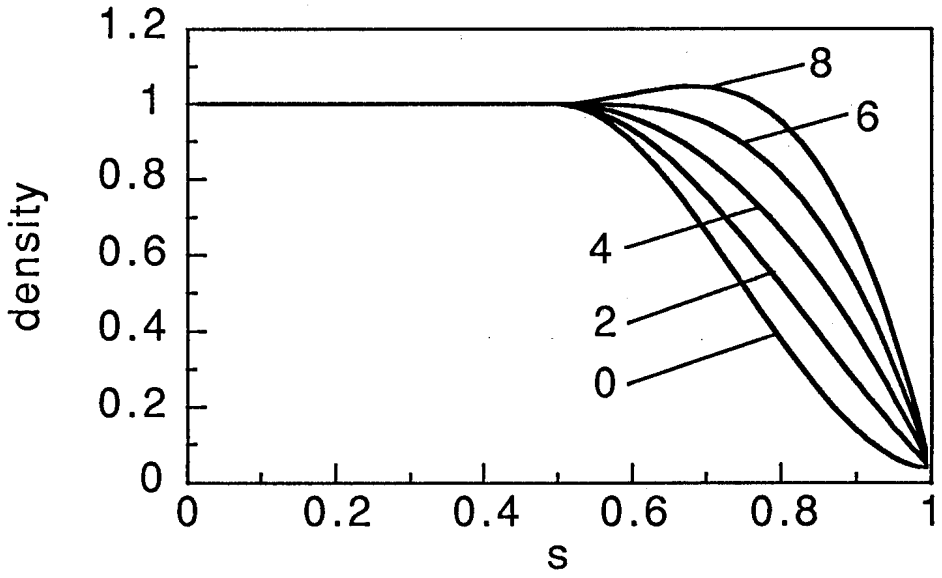
1.2
1
0.8
0.6
0.4
0.2
0
density
0
0.2
0.4
0.6
0.8
1
s
8
6
4
2
0

FIG.1

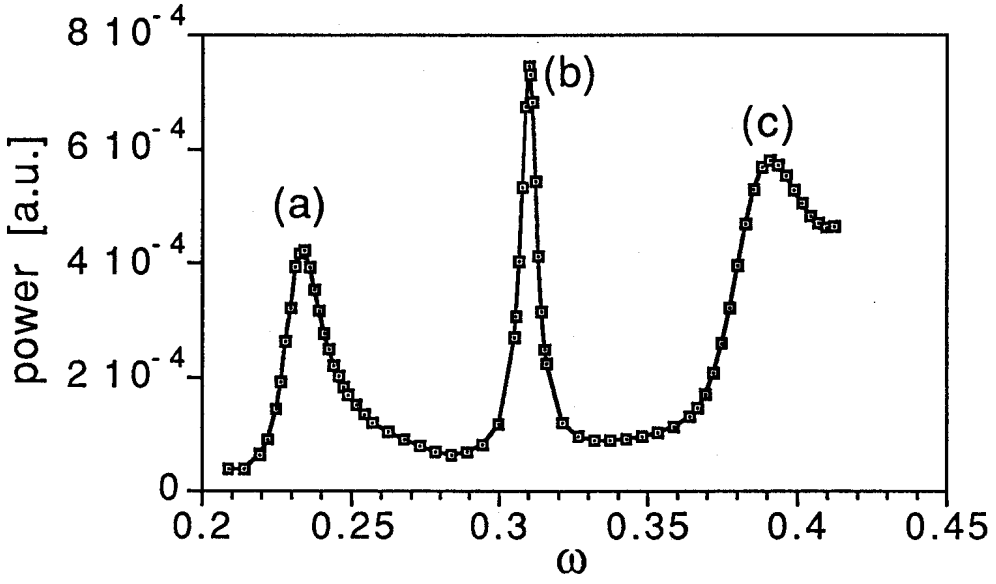
8 10-4
6 10-4
4 10-4
2 10-4
0
power [a.u.]
0.2
0.25
0.3
0.35
0.4
0.45
ω
(a)
(b)
(c)

FIG. 2

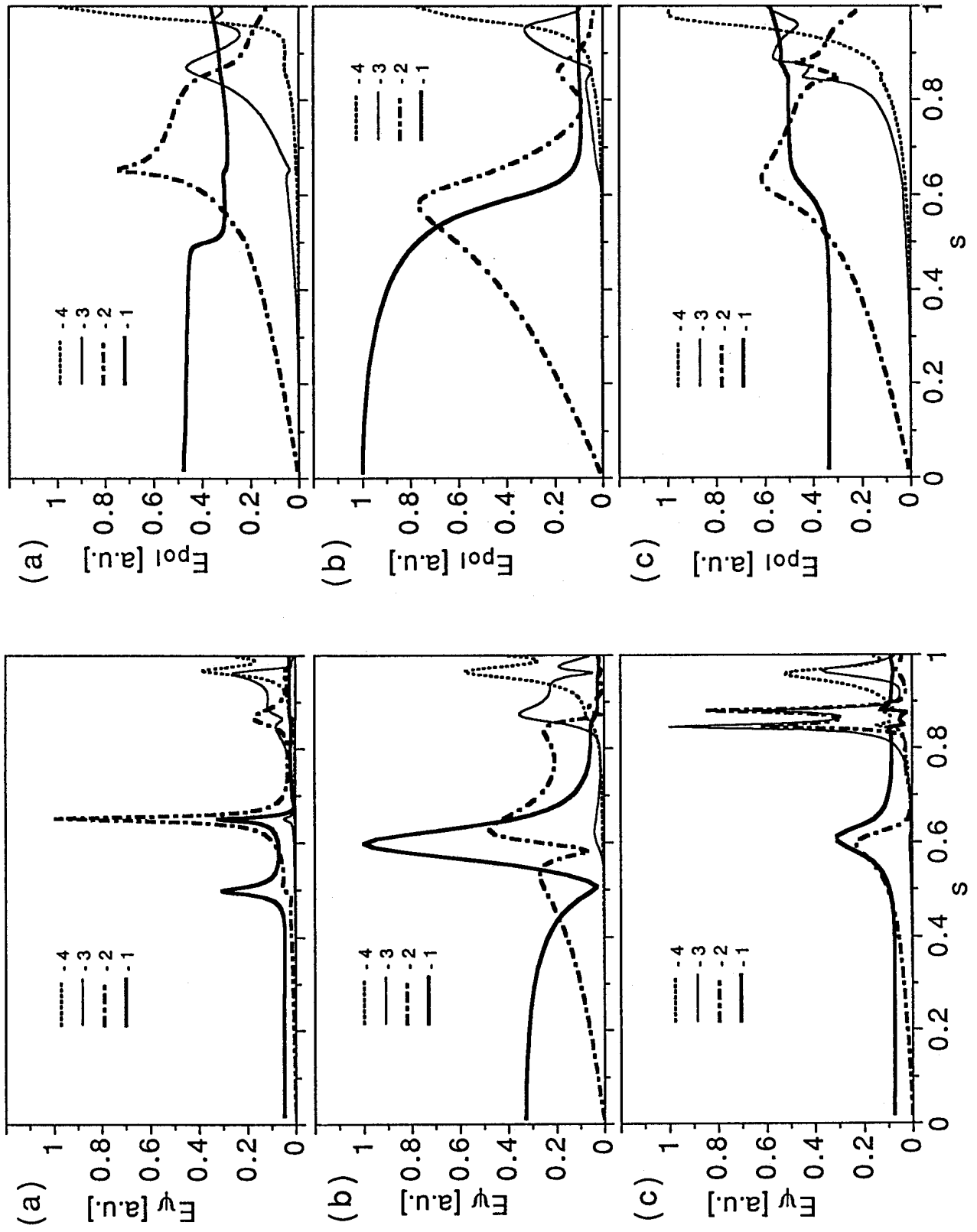

FIG.4

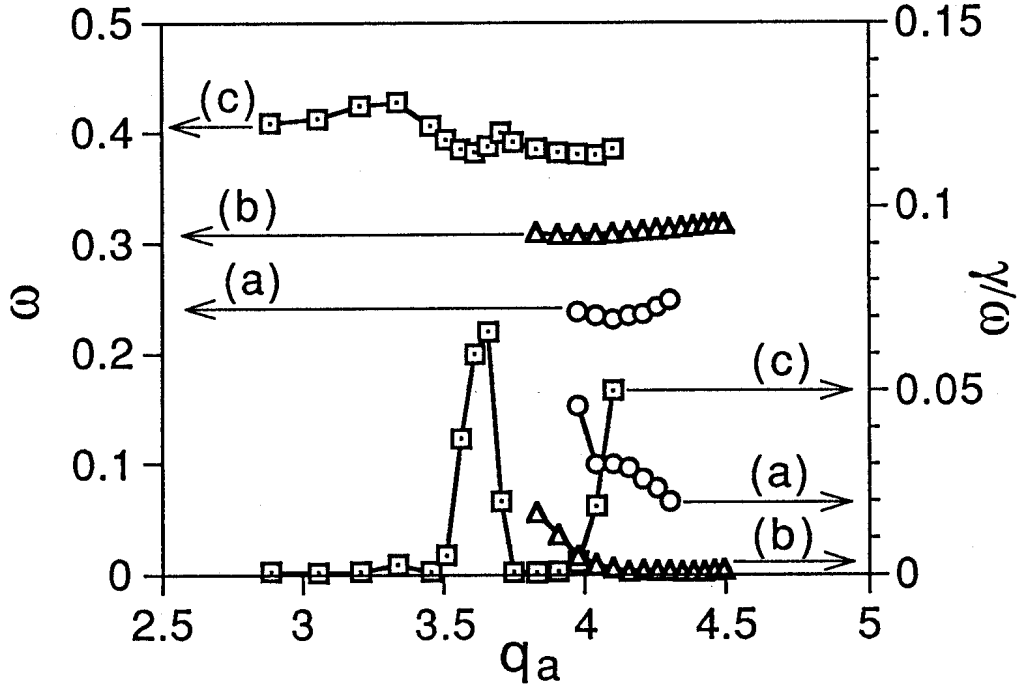
0.5
0.4
0.3
0.2
0.1
0
ω
0.15
0.1
0.05
0
γ/ω
(c)
(b)
(a)
(c)
(a)
(b)
2.5
3
3.5
4
4.5
5
qa

FIG. 5

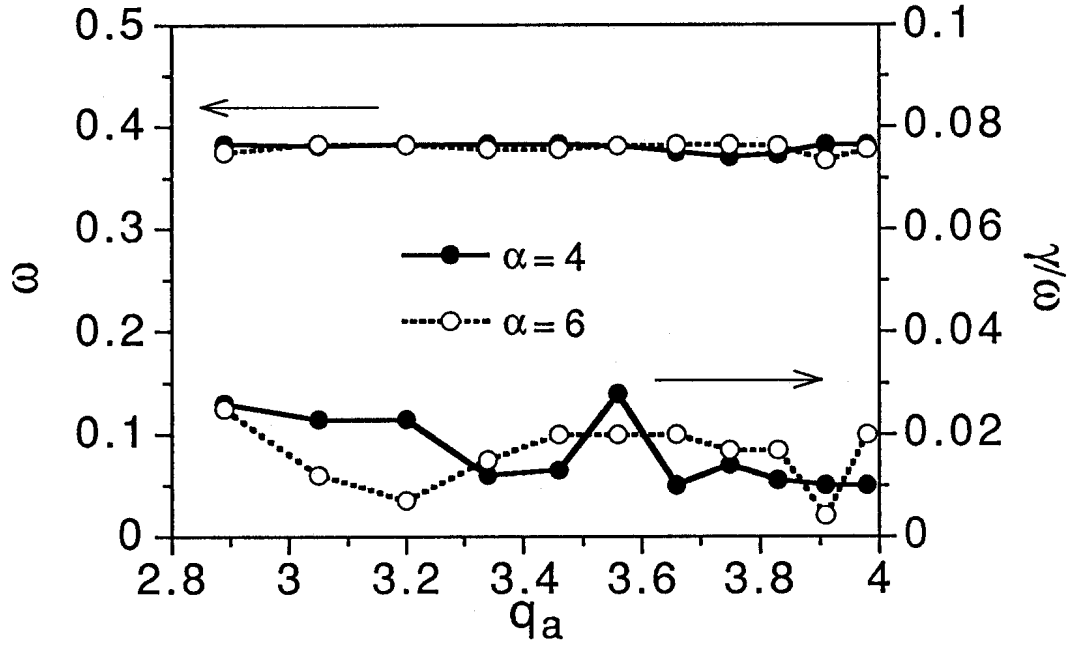
0.5
0.4
0.3
0.2
0.1
0
ω
0.1
0.08
0.06
0.04
0.02
0
γ/ω
α = 4
α = 6
2.8
3
3.2
3.4
3.6
3.8
4
qa

FIG. 6

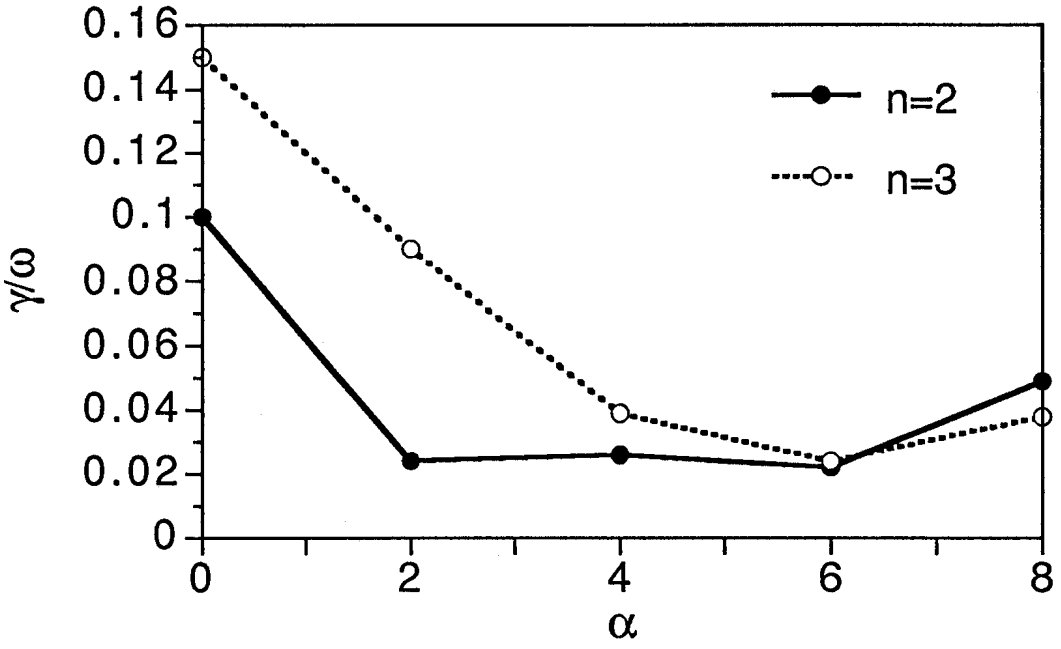

FIG.7

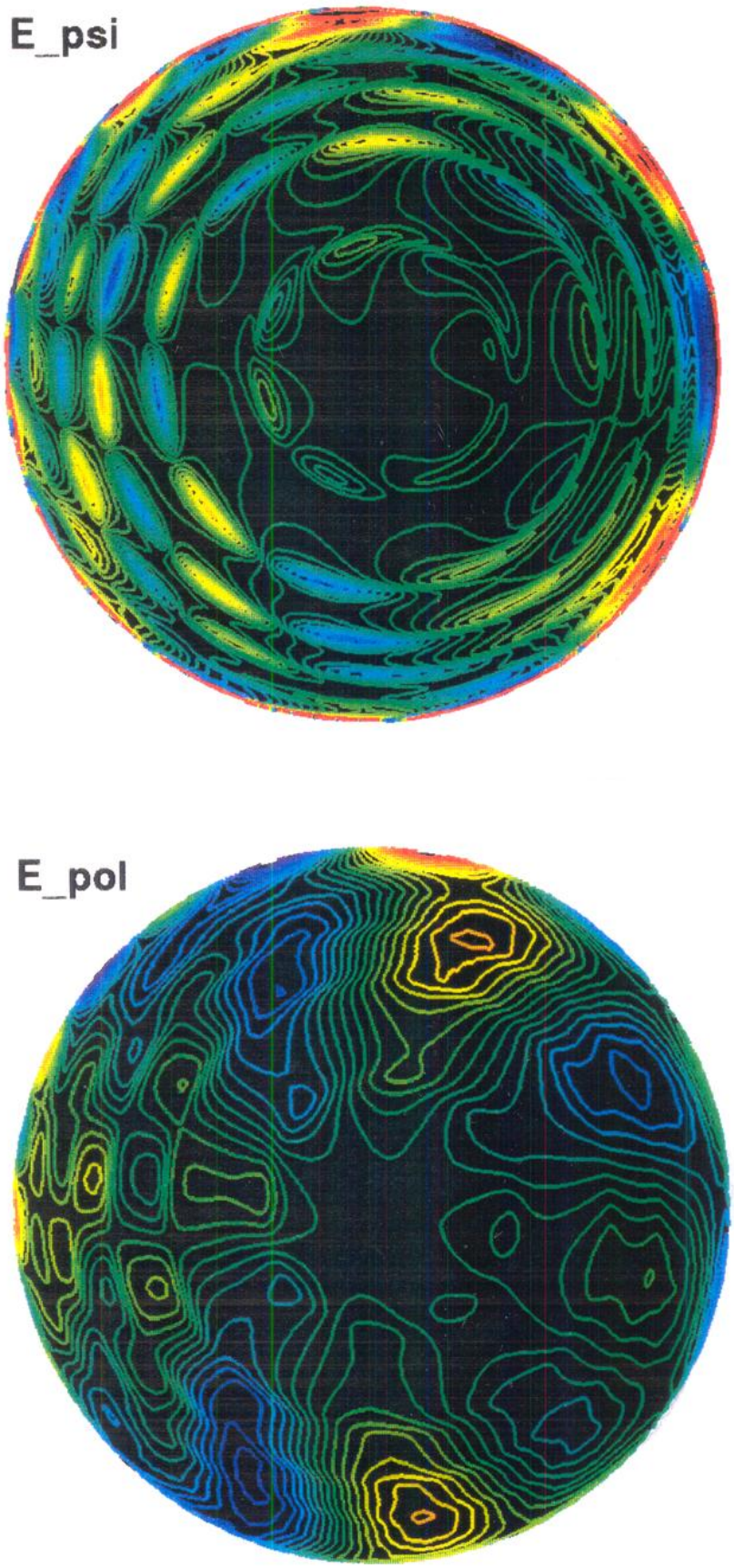

FIG.8

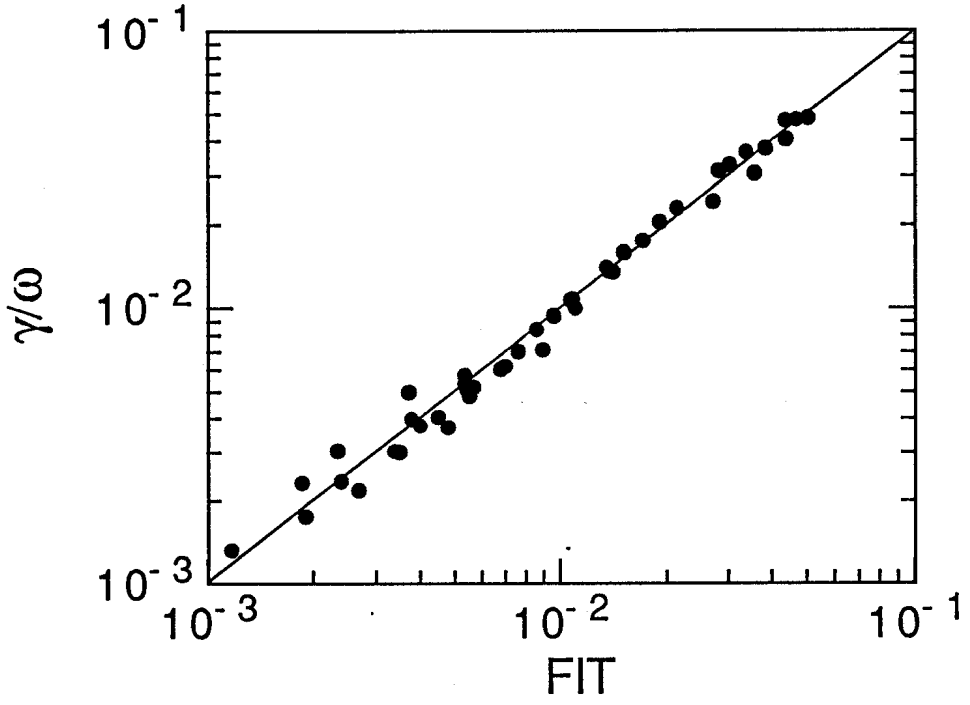

FIG.9

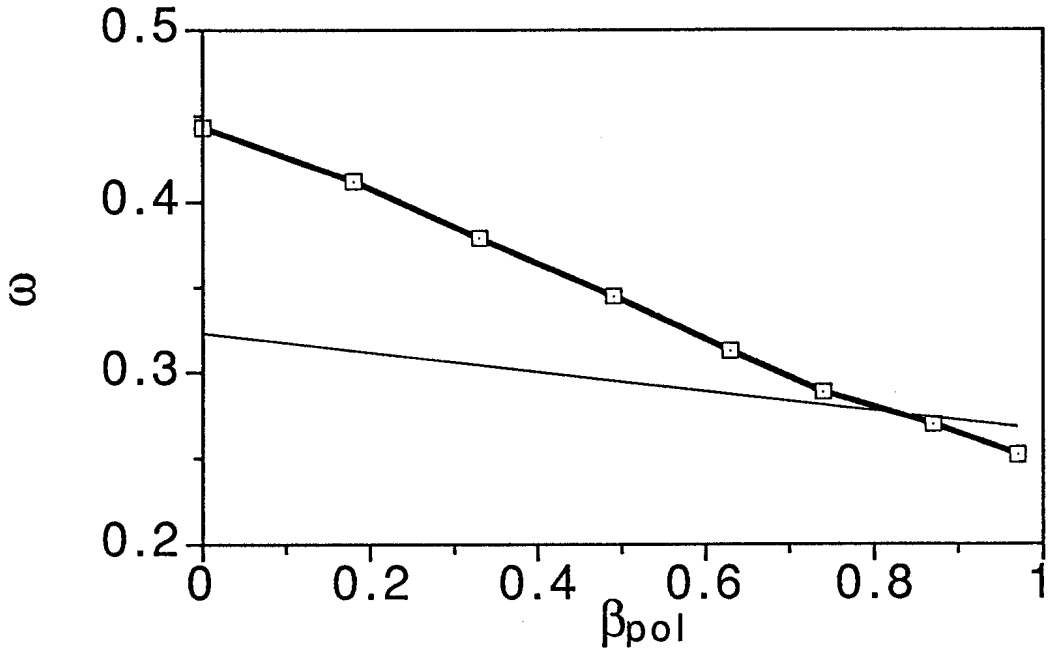

FIG.10

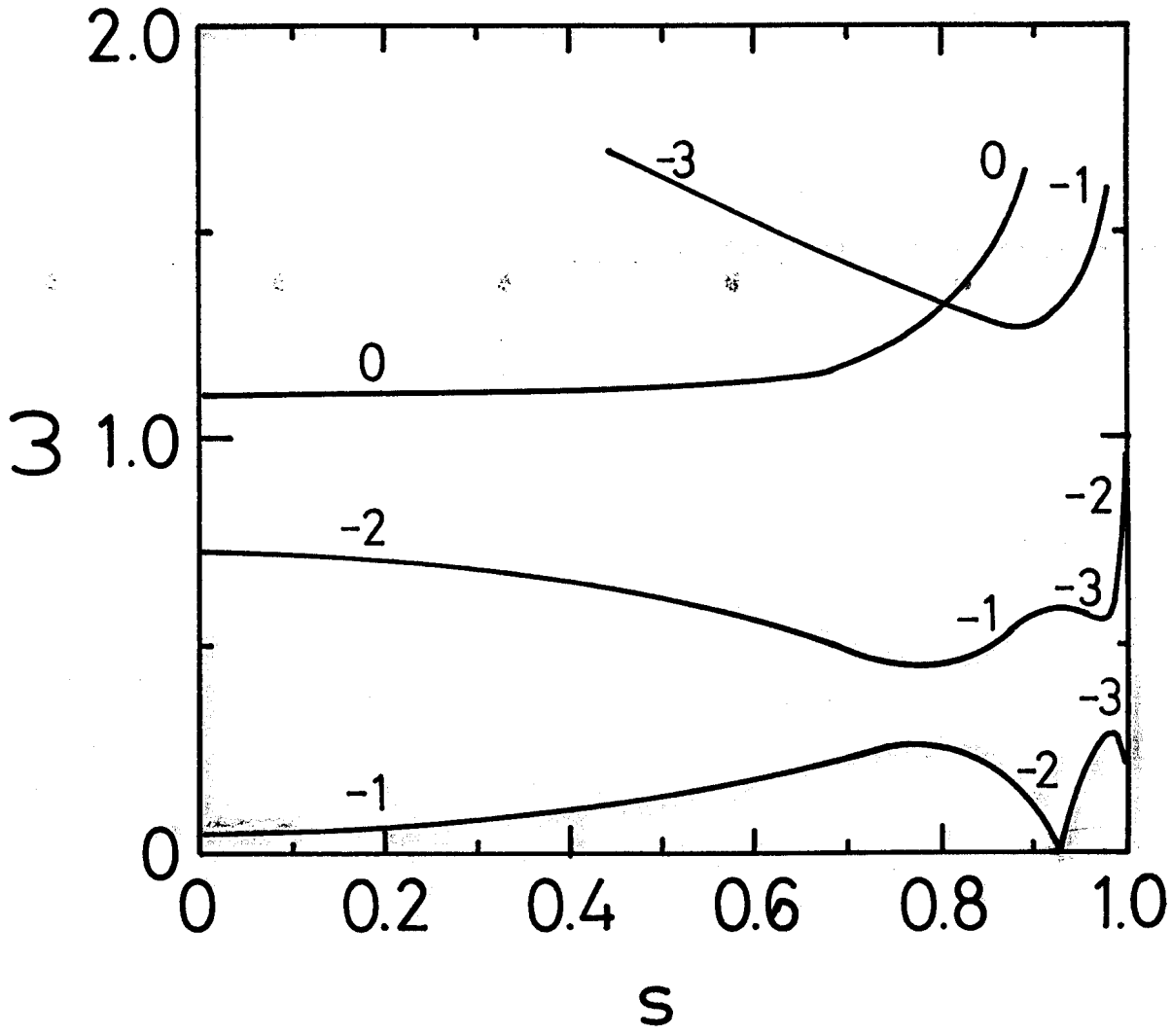

FIG.11

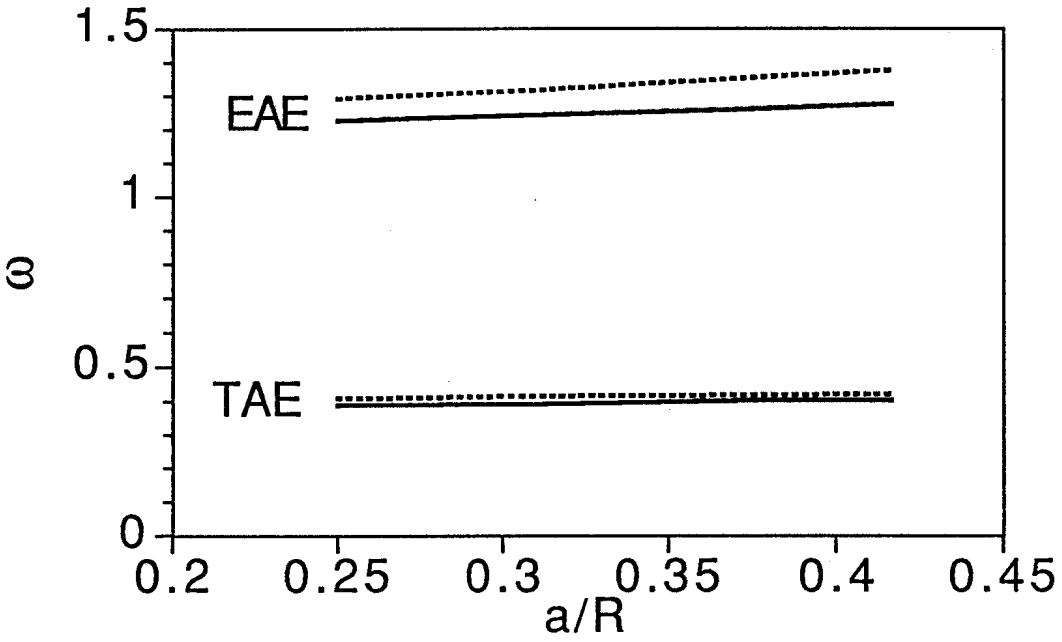
1.5
1
0.5
0
ω
EAE
TAE
0.2
0.25
0.3
0.35
0.4
0.45
a/R

FIG.12

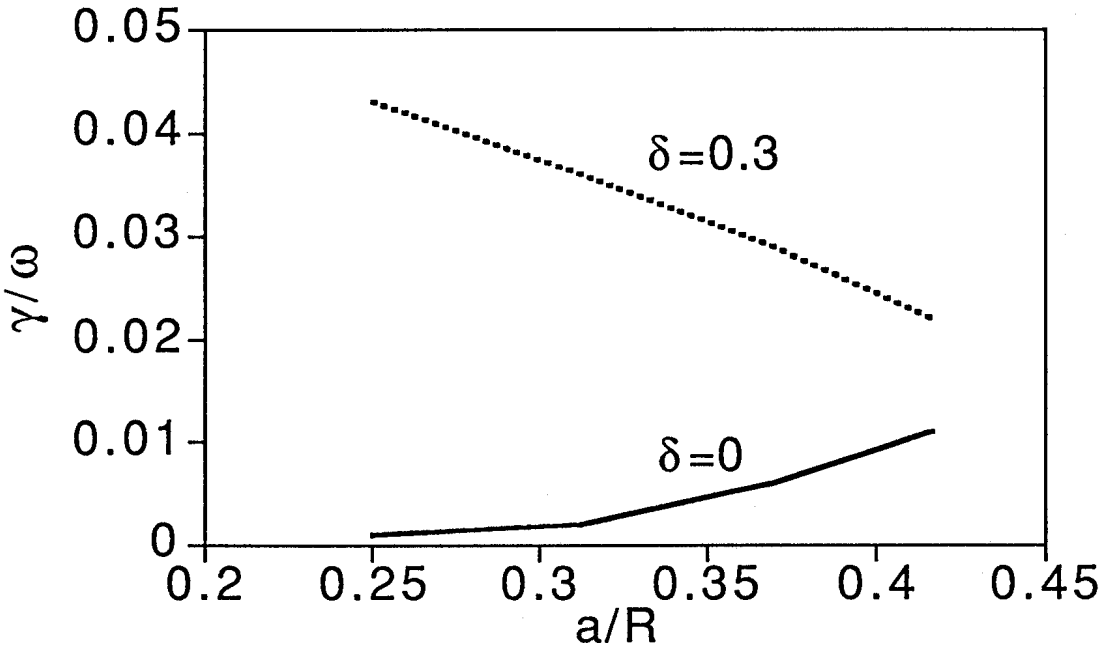
0.05
0.04
0.03
0.02
0.01
0
γ/ω
δ=0.3
δ=0
0.2
0.25
0.3
0.35
0.4
0.45
a/R

FIG.13

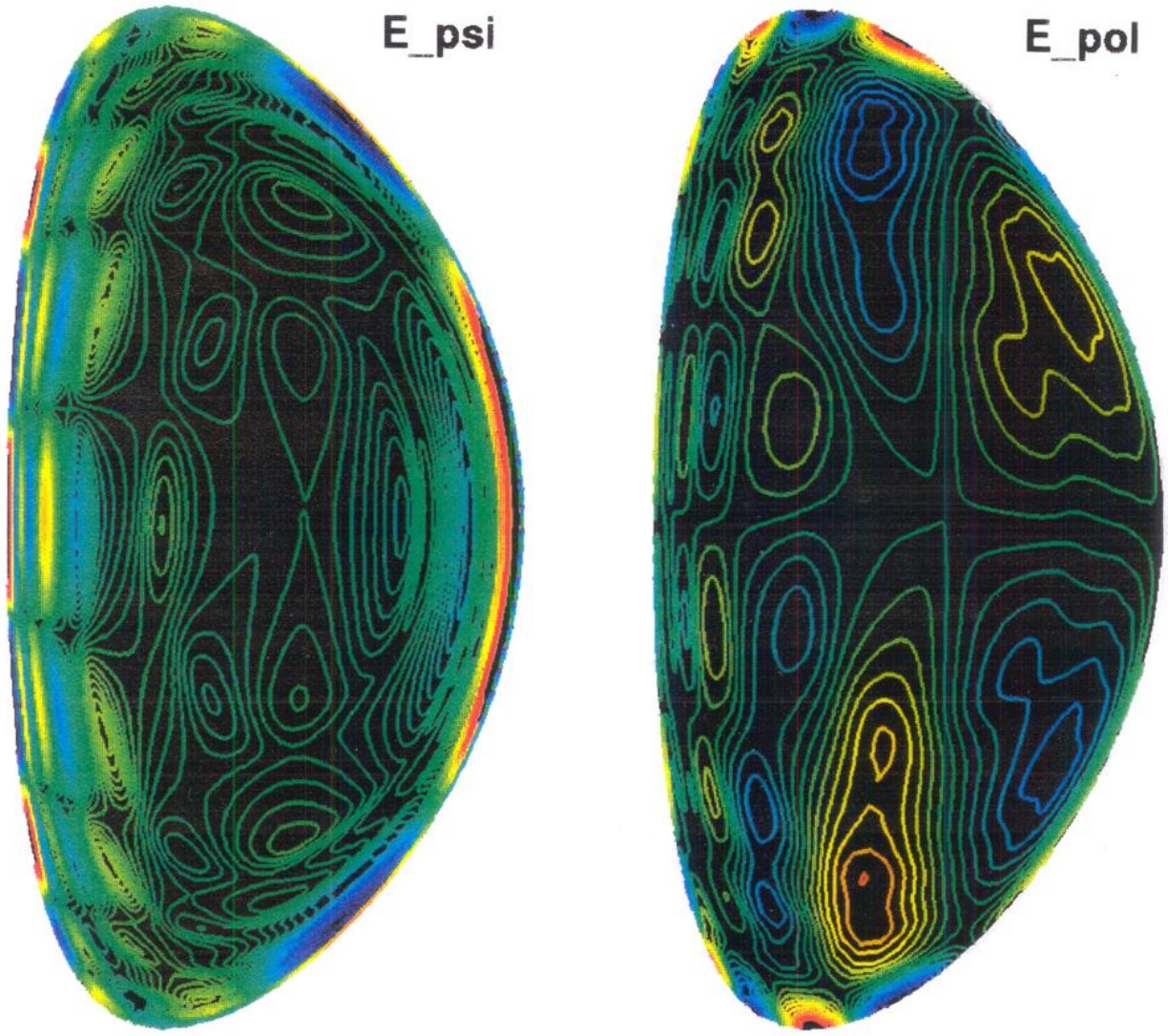

FIG. 14

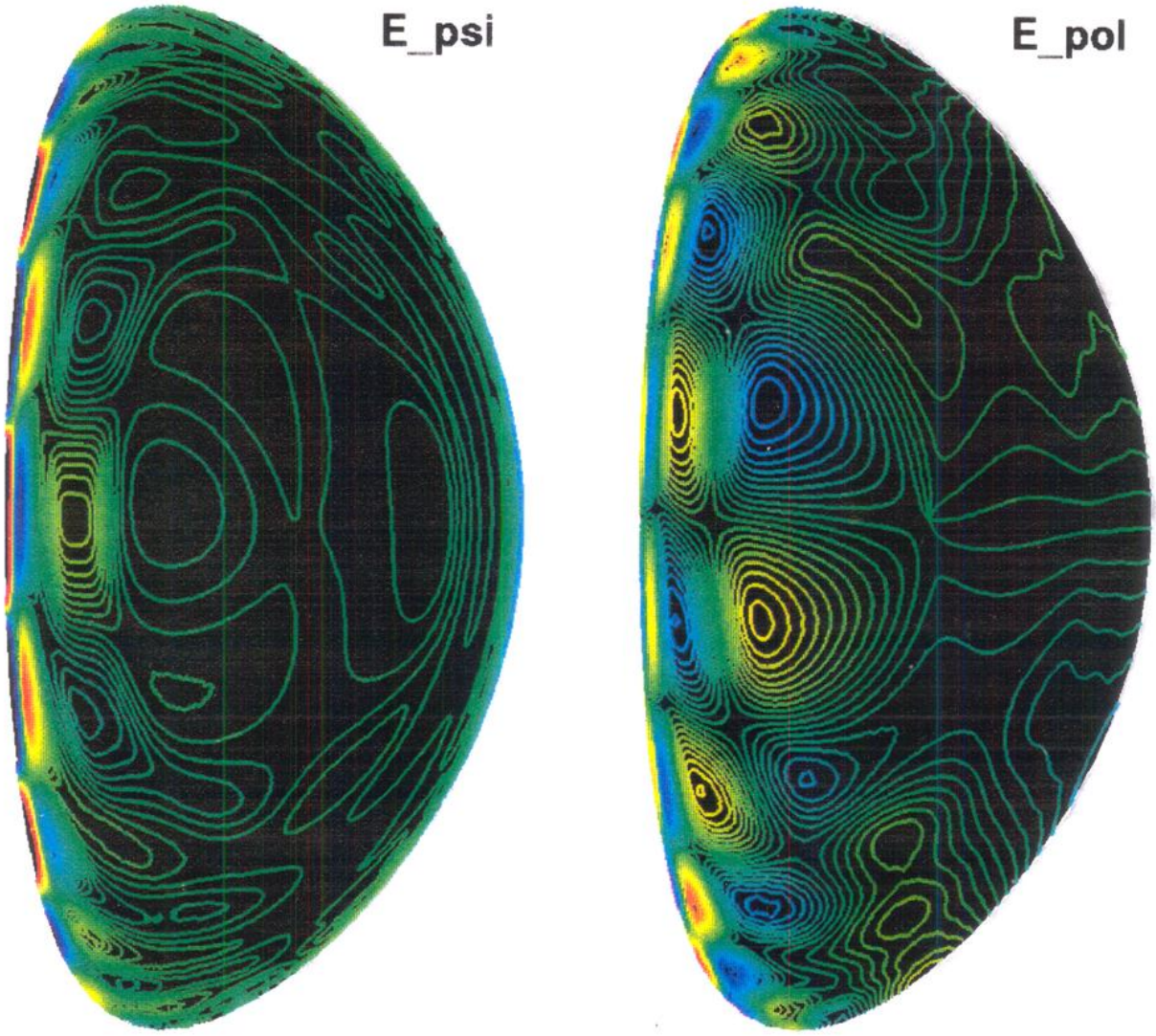

FIG. 15

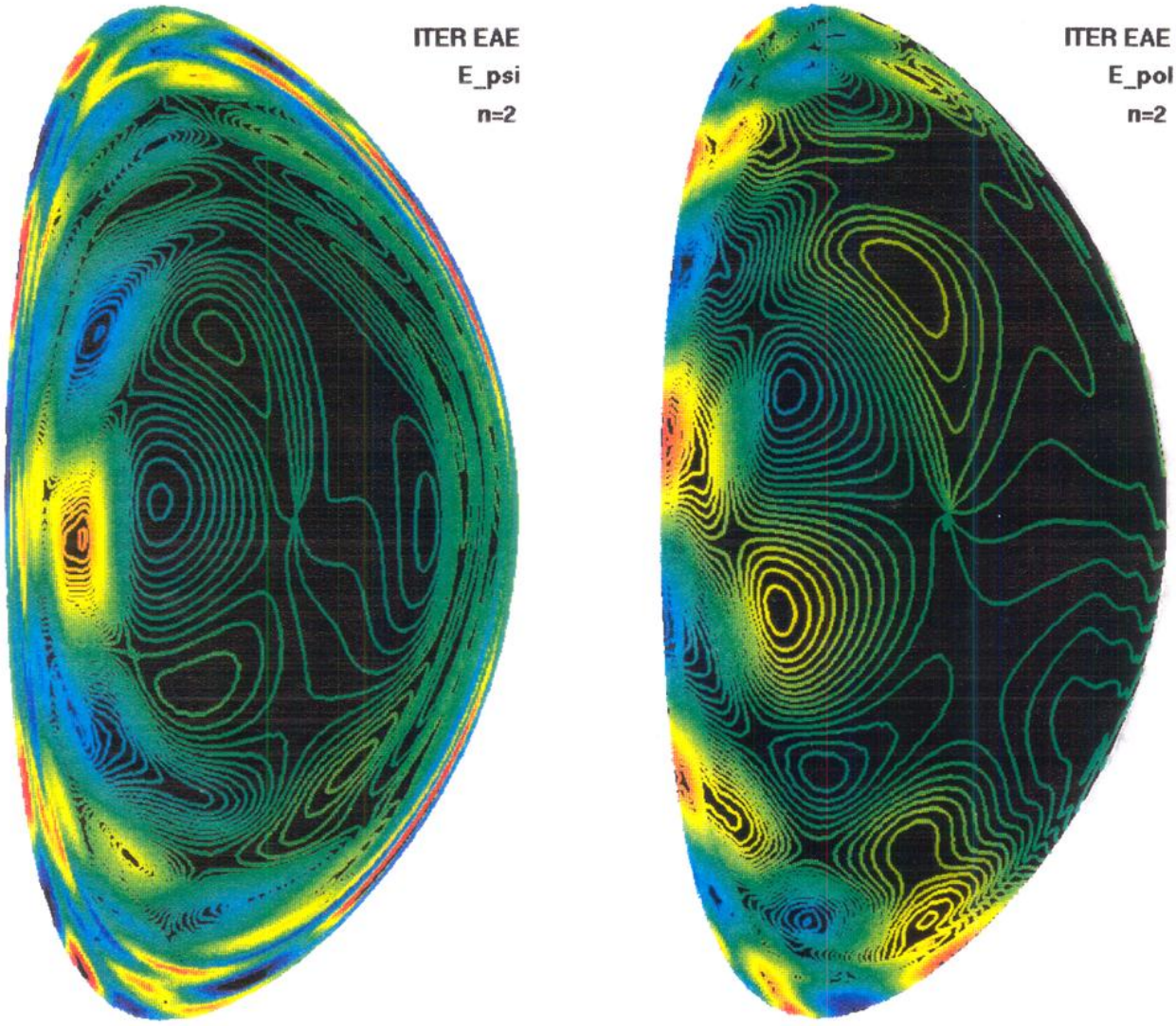

FIG.16